Integrin α5-PDE4D Interaction Regulates Endothelial Inflammatory Signaling

Sanguk Yun[1], Madhusudhan Budatha[1], James E. Dahlman[2,3,4], Brian G. Coon[1], Ryan T. Cameron[5], Robert Langer[2,3,4,6], Daniel G. Anderson[2,3,4,6], George Baillie[5] and Martin A. Schwartz[1,7,8,*]

[1]Department of Internal Medicine, Yale Cardiovascular Research Center, Yale University, New Haven, CT 06520, USA

[2]David H. Koch Institute for Integrative Cancer Research, Massachusetts Institute of Technology, Cambridge, MA 02139, USA

[3]Harvard-MIT Division of Health Sciences and Technology, Massachusetts Institute of Technology, Cambridge, MA 02139, USA

[4]Institute for Medical Engineering and Science, Massachusetts Institute of Technology, Cambridge, MA 02139, USA

[5]Institute of Cardiovascular and Medical Science, College of Medical, Veterinary and Life Sciences, University of Glasgow, Glasgow G12 8QQ, Scotland, UK

[6]Department of Chemical Engineering, Massachusetts Institute of Technology, Cambridge, MA 02139, USA

[7]Department of Biomedical Engineering, Yale University, New Haven, CT 06520, USA

[8]Department of Cell Biology, Yale University, New Haven, CT 06520, USA

*Correspondence: martin.schwartz@yale.edu

The authors have declared that no conflict of interest exists.

Abstract

Atherosclerosis is primarily a disease of lipid metabolism and inflammation, however, it is also closely associated with endothelial extracellular matrix (ECM) remodeling, with fibronectin accumulating in the laminin-collagen basement membrane. To investigate how fibronectin modulates inflammation in arteries, we replaced the cytoplasmic tail of the fibronectin receptor integrin α5 with that of the collagen/laminin receptor integrin α2. This chimera suppressed inflammatory signaling in endothelial cells on fibronectin and in knock-in mice. Fibronectin promoted inflammation by suppressing anti-inflammatory cAMP. cAMP was activated through endothelial prostacyclin secretion, however, this was ECM-independent. Instead, cells on fibronectin suppressed cAMP via enhanced phosphodiesterase (PDE) activity, through direct binding of integrin α5 to phosphodiesterase-4D5 (PDE4D5), which induced PP2A-dependent dephosphorylation of PDE4D5 on the inhibitory site Ser561. *In vivo* knockdown of PDE4D5 inhibited inflammation at athero-prone sites. These data elucidate a molecular mechanism linking ECM remodeling and inflammation, thereby identifying a new class of therapeutic targets.

Introduction

Atherosclerosis is an inflammatory disease of large to mid-sized arteries that is strongly linked to lipid metabolism [1]. Current concepts and clinical approaches focus mainly on these aspects. However, atherosclerotic plaques occur mainly in regions of arteries with disturbed flow [2, 3], which triggers oxidative stress, activation of NF-κB and other mediators, endothelial inflammatory gene expression, and leukocytes recruitment [4]. These local influences synergize with systemic risk factors such as high plasma LDL-cholesterol and triglycerides, hypertension, diabetes or smoking, to induce atherosclerotic plaques [5].

Inflammation and ECM remodeling are closely associated across many biological systems and disease processes [6-8]. Inflammation induces ECM remodeling, with increases in provisional ECM proteins such as fibronectin, osteopontin and fibrin. Conversely, ECM proteins and fragments modulate inflammatory processes. These complex interactions between ECM and inflammatory pathways contribute to normal developmental and adult remodeling, and to a variety of pathologies.

In stable, unperturbed vessels, the subendothelial basement membrane consists mainly of collagen IV, laminin and associated proteoglycans with minimal fibronectin (FN) [9]. By contrast, fibronectin expression and matrix assembly are upregulated during development, angiogenesis and flow-dependent vessel remodeling [10-12]. FN is also deposited in the intima at atheroprone regions of arteries [13]. This occurs even in athero-resistant WT mice, associated with endothelial inflammatory gene expression, indicating that it is an early event. FN increases in hypercholesterolemic mice together with atherosclerotic plaque progression. Studies in genetically modified mice support a causal role for FN in atherosclerosis [14-16].

In vitro studies with endothelial cells (ECs) showed that disturbed flow or acute changes in flow activates inflammatory pathways such as NF-κB, and induces expression of leukocyte

recruitment molecules such as ICAM-1, MCP-1 and VCAM-1[17, 18]. However, these events depend strongly on the ECM proteins to which the ECs adhere: cells on collagen I or IV, or basement membrane protein (matrigel) suppress NF-κB, JNK and PAK in response to flow and soluble inflammatory mediators but are activated in ECs on FN [13, 19-21]. Selective activation of cAMP and protein kinase A (PKA) in cells on collagen or basement membrane protein relative to FN mediates the suppression of inflammatory pathways [22,23]. But how different integrins control cAMP/PKA and inflammation is unknown.

The major fibronectin receptor, α5β1, and the major collagen/laminin receptor, α2β1, that are strongly implicated in pro- vs. anti-inflammatory signaling *in vitro* and *in vivo* [24, 25] share the common β1 subunit. While α2β1 binds best to fibrillar collagens, it also serves as a functionally relevant receptor for collagen IV and laminins [26]. We therefore hypothesized that the cytoplasmic domains of the unique integrin alpha subunits may determine differential inflammatory signaling. In this study, we examined chimeric in which the cytoplasmic tail of integrin α5 was replaced by that of α2. Our results show that ECM-dependent differential inflammatory signaling is due to an interaction of the α5 cytoplasmic domain with the cAMP-specific phosphodiesterase PDE4D5, with consequent regulation of PDE4D5 phosphorylation, likely by protein phosphatase 2A (PP2A).

Results

An integrin α5/2 chimera blocks flow-dependent inflammatory signaling

To examine ECM-specific signaling, we constructed a chimeric integrin in which the α5 cytoplasmic tail was replaced with the α2 tail (Fig. 1a). When over-expressed in bovine aortic endothelial cells (BAECs) the integrin α5/2 chimera localized to the cell surface (Fig. S1a) and hetero-dimerized with the integrin β1 subunit similarly to wild type (Fig. S1b). Chimera-

expressing BAECs adhered and spread normally on FN (Fig. S1c, Fig. 2d, e), and showed normal FAK activation, FN fibrillogenesis and alignment in laminar flow (Fig. S1d, e, f). We then investigated shear-dependent inflammatory responses. The critical inflammatory transcription factor NF-κB shows transient activation by onset of flow, and sustained activation by oscillatory flow [27, 28]. In both cases, the α5/2 chimera blocked NFκB activation (Fig. 1b, c) and expression of the NFκB target gene ICAM-1 (Fig. 1d). We also noted that the α5/2 chimera gave somewhat higher basal activation of NF-κB and other inflammatory pathways, but this also occurs with normal ECs on collagen or basement membrane protein [13, 21]. While this feature has not been further investigated, the combined results demonstrate that the α5/2 chimera phenocopies cells on basement membranes.

ECM also modulates endothelial responses to soluble inflammatory mediators [19, 24]. IL-1β and oxidized LDL are two critical inflammatory mediators in atherosclerosis that also activate NF-κB. IL-1β and oxidized LDL strongly activated NF-κB in control ECs on FN, whereas control cells on matrigel, or α5/2 chimera cells on FN were largely resistant (Fig. 1e-g). Previous results showed that selective activation of the cAMP/PKA pathway suppressed NF-κB on coll IV-laminin basement membranes [22]. Shear stress activated PKA in cells expressing the α5/2 chimera but not WT α5 on FN (Fig. 1h). Furthermore, blocking PKA with PKI 14-22 amide, a cell permeable PKA inhibitor, restored NF-κB activity in chimera-expressing cells (Fig. 1i). Together, these data show that differential PKA activation and subsequent inflammatory responses are mediated by the integrin α tails.

Integrin chimera knock-in mice

To investigate the role of integrin α tails *in vivo*, we made knock-in mice in which the exon encoding the endogenous integrin α5 cytoplasmic domain was replaced with that of integrin α2

following Cre-mediated recombination (Fig. 2a). Breeding of α5/2-floxed-neo mice with CMV-Cre TG mice resulted in replacement of WT integrin α5 with the α5/2 chimera (Fig. 2b, c). These mice were viable and able to reproduce. A complete analysis of these mice will be reported elsewhere; in this study, we focused on endothelial phenotype. To confirm functionality, ECs isolated from WT and knock-in mice were plated on FN. The α5/2 cells showed no differences in adhesion or spreading (Fig. 2d, e), confirming normal function. Endothelial inflammatory activation marked by elevated expression of fibronectin, ICAM-1 and VCAM-1 occurs in regions of disturbed flow in wild type C57Bl6 mice [13] and is a strong marker for susceptibility to atherosclerosis [29, 30]. Staining for these proteins in the athero-prone inner curvature of the aortic arch was greatly reduced in integrin α5/2 knock-in mice (Fig. 2f). Thus, the integrin α5/2 chimera suppresses flow-dependent early inflammation *in vivo*.

PGI_2 mediates flow-dependent cAMP-PKA activation

We next addressed how the ECM-integrin interaction modulates flow-dependent cAMP-PKA activation. The pathway by which flow activates cAMP and PKA is unknown, however, flow can induce PGI_2 (prostacyclin) secretion in ECs [31], which binds a Gs-coupled receptor to activate adenylate cyclase and induce cAMP production [32], which promotes vasodilation and inhibits thrombosis and inflammation [33]. To test this pathway, HUVECs on matrigel were subject to flow with or without the cyclooxygenase (COX) inhibitor aspirin to block PGI_2 synthesis, or the PGI_2 receptor antagonist RO1138452 to block PGI_2 signaling. Both of these treatments efficiently inhibited shear stress-dependent PKA activation (Fig. 3a). They also conferred NFκB activation by flow in cells on matrigel (Fig. 3b, c), confirming the importance of PKA in suppressing inflammatory pathways. Similarly, in α5/2 chimera cells on FN, blocking prostacyclin synthesis (with indomethacin) or the PGI_2 receptor inhibited flow-induced PKA activation (Fig. 3d) and

conferred NF-κB activation (Fig. 3e, f). Thus, suppression of NF-κB by adhesion of cells to basement membranes is mediated by prostacyclin and its receptor.

Next, to test whether shear stress-dependent PGI_2 secretion is ECM-specific, we analyzed the stable prostacyclin metabolite 6-keto-PGF1α, an approach that circumvents the instability of PGI_2. Flow greatly increased 6-keto-PGF1α production, consistent with published data [31, 34]. However, 6-keto-PGF1α levels did not differ between FN and matrigel (Fig. 3g). Thus, prostacyclin production cannot account for the difference in cAMP and PKA activation in cells on different matrices.

PDE4D is required for ECM-specific NFκB activation

We next considered whether differential cAMP degradation might mediate the observed ECM specificity. Phosphodiesterases (PDEs) are the enzymes that hydrolyze cAMP to reduce or terminate signaling [35, 36]. We focused on the PDE4 family, which are abundant in endothelial cells [37-40]. We reasoned that if PDE4 is critical, its inhibition should restore PKA activation in endothelial cells on FN to levels similar to those on collagen or basement membranes. We first tested the PDE4 inhibitor rolipram, which increased shear-dependent PKA activation in cells on FN (Fig. 4a) and abolished flow-dependent NFκB activation, without affecting NFκB activity on collagen (Fig. 4b). By contrast, flow-dependent AMPK activation was unaffected by ECM or rolipram (Fig. S2a). PDE4 compartmentalization by protein-protein interactions mediates functional specificity in many systems [41]. Among the PDE4 sub-families, both PDE4C and PDE4D were reported in endothelial cells [42]. The PDE4D subfamily has eleven splicing variants, however, we used a panPDE4D antibody and a PDE4D5-specific antibody to show that PDE4D5 is the only isoform detected in HUVEC and BAEC cells (Fig. S2b).

We next examined whether PDE4D5 associates with integrins. Immunoprecipitation of endogenous PDE4D5 from HUVECs with two different antibodies brought down α5 but not α2

integrin (Fig. 4c). Immunoprecipitating WT α5 or the α5/2 chimera showed that this interaction required the α5 cytoplasmic domain (Fig. 4d). To investigate PDE4D function in flow-dependent NFκB activation, we performed knock-down and reconstitution experiments. PDE4D knock-down almost completely abolished shear stress-dependent NFκB activation in cells on FN, which was rescued by an siRNA-resistant construct (Fig. 4e). To test whether targeting PDE4D5 to focal adhesion is sufficient for these effects, we fused the focal adhesion targeting domain of FAK to PDE4D5 [43]. This construct strongly localized to focal adhesions in cells on matrigel (Fig. S2c) and conferred flow-induced NFκB activation (Fig. 4f). This construct also reduced shear stress-dependent Creb phosphorylation, confirming suppression of PKA activity.

Direct interaction between the PDE4D5 UCR2 linker and integrin α5

We next mapped the integrin binding region in PDE4D5 using bacterially expressed and purified fragments of PDE4D5 (Fig. 5a) to pull down integrin α5 from cell lysates. Binding was observed only with the regulatory upstream conserved region 2 (UCR2) with flanking connecting segments (Fig. 5b). Using purified integrin α tail fusion proteins that form coiled coil domain-mediated homo-dimers [44], only integrin α5 bound the purified PDE4D5 F2 fragment, indicating that the association is direct and specific (Fig. 5c). Examining a series of deletions (Fig. 5d) showed that the C-terminal 13 amino acids from GST-F1-F2 is required for the interaction (Fig. 5e). Among those 13 amino acids, mutation of $K^{292}KKR^{295}$ to either EEEE or AAAA completely blocked, and single amino acid substitutions partially blocked the interaction (Fig. 5f). Thus, a short, basic sequence in the connecting segment between UCR2 and the catalytic domain is required for binding integrin α5.

To further validate this interaction, cells expressing WT or mutated GFP-PDE4D5 were plated on fibronectin or collagen, then subject to flow for 15 min. In cells on FN, WT PDE4D5 but not PDE4D5 with a mutated α5 binding sequence co-localized with the focal adhesion marker

vinculin; co-localization was also lost in cells on collagen (Fig. 5g). Thus, the interaction with α5 specifically recruits PDE4D5 to focal adhesions.

Integrin α5 binding is required for NF-κB activation on fibronectin

To address whether the interaction between integrin α5 and PDE4D5 is required for pro-inflammatory signaling in cells on FN, we reconstitution PDE4D5 knock-down cells with WT or mutant PDE4D5. Whereas the WT PDE4D5 construct recovered NFκB activation, 4E and 4A mutants were inactive, as was catalytically dead PDE4D5 (D556A) (Fig. 5h). Thus, PDE4D binding to integrin α5 and catalytic activity are required for inflammatory signaling. Together, these results show that recruitment of PDE4D5 to focal adhesions via α5 binding mediates its pro-inflammatory function by suppressing anti-inflammatory PKA activation.

Regulation of PDE4D phosphorylation by integrin α5

We then considered whether localization of PDE4D5 by integrin α5 is the sole determinant of these effects or whether PDE4 catalytic activity is affected. Assaying catalytic activity of purified PDE4D *in vitro* after addition of recombinant integrin α5 tails revealed no changes. PDE4D5 activity is also regulated by phosphorylation; one important site is S651, which can be phosphorylated by Erk and suppresses enzymatic activity [45]. Western blotting with an antibody to this site showed that S651 phosphorylation increased in cells on collagen compared to FN, independent of fluid shear stress. Further, the reduced phosphorylation on FN was lost in the 4E mutant (Fig. 6a). Cells expressing the chimeric integrin α5/2 plated on FN also showed high S651 PDE4D phosphorylation compared to WT α5 cells (Fig. 6b). These data suggest either that the integrin α5-PDE4D interaction suppresses S651 phosphorylation or that integrin α2 activates it. Analysis of cells expressing wild type or 4E mutant PDE4D5 were analyzed in suspension or after adhesion to FN-coated dishes. Plating on FN triggered S651 dephosphorylation in wild type PDE4D5 but not the 4E mutant (Fig. 6c). Chimeric integrin α5/2

also failed to trigger S651 dephosphorylation on FN (Fig. 6c). Thus, binding to integrin α5 in cells on FN induces PDE4D5 S651 dephosphorylation.

Proteomic analysis revealed PP2A in PDE4D5 immunoprecipitates in ECs on FN (Fig. S3a). Co-immunoprecipitation confirmed this interaction in cells on FN but not matrigel (Fig. S3b). Both the PP2A inhibitor okadaic acid (OA) and siRNA against the PP2A catalytic subunit blocked FN-dependent S651 dephosphorylation after plating on FN (Fig. S3c) and in stable monolayers (Fig. S3d, e) without affecting endothelial cell adhesion, spreading or FAK activation on FN (Fig. S4a, b). However, these treatments efficiently blocked NF-κB activation by flow and IL1β on FN (Fig. S3f, g).

We next addressed whether S651 phosphorylation controls ECM-specific NFκB activation. For ECs on collagen, expression of phospho-resistant S651A mutant in PDE4D knock-down cells increased NF-κB activity (Fig. 6d). Conversely, in cells on FN, rescue of PDE4D5 knock down with phospho-mimetic S651E mutant failed to restore NFκB activation (Fig. 6e). These results show that control of PDE4D5 phosphorylation on S651 by integrins determines subsequent inflammatory signaling.

Endothelial specific knock-down of PDE4D inhibits inflammation

We next investigated whether PDE4D is required for flow-dependent inflammatory activation of the endothelium *in vivo* using siRNA. For these experiments, we used recently developed nano-particles that are highly specific to ECs and do not knock-down genes in hematopoietic cells, including leukocytes, or in hepatocytes, even at a high dose (2.0 mg/kg)[46]. We first screened multiple siRNAs and identified a sequence that depleted mouse PDE4D *in vitro* with an IC_{50} of 0.05 nM (Fig. S5a), which is ~100x lower than most siRNAs. Transfection into cultured mouse ECs abolished flow-dependent NF-κB activation and ICAM-1 induction, which was rescued by viral expression of human PDE4D5 (Fig. 7a), thus, confirming the efficacy and specificity of this

siRNA sequence. A version of this siRNA was chemically modified to improve stability and packaged into nanoparticles, then injected intravenously into mice (1.0 mg/kg). Isolation of aortic endothelial mRNA 14 days after injection showed a ~70% decrease in PDE4D mRNA compared to the luciferase control siRNA (Fig. S5b). C57BL6 mice were then injected three times in a month with PDE4D or luciferase siRNA nanoparticles. The PDE4D siRNA greatly reduced inflammatory gene expression in an atheroprone artery segment compared to luciferase siRNA (Fig. 7b).

Effects on atherosclerosis

Lastly, we investigated atherosclerosis in the integrin α5/2 chimeric mice by breeding onto the hypercholesterolemic ApoE$^{-/-}$ background, which, on a high fat, "Western" diet, develop atherosclerotic plaques at regions of disturbed flow, similar to human disease [47]. Aortas from these mice after 4 months on a high fat diet showed dramatically decreased plaque burden (Fig 7c). These results validate the connection between early inflammatory activation of the endothelium by disturbed shear and later disease progression in hyperlipidemia.

Discussion

Inflammation has frequently been described as a double edged sword that is required for tissue defense, remodeling and repair but, if not properly regulated, causes damage or disease [48, 49]. Inflammatory reactions therefore need to be initiated upon infection, injury or stress, but then resolved when the infection is cured, injury healed or stress relieved. Linking the biochemical and structural changes associated with tissue repair and remodeling with the pathways that govern inflammation appears to be essential for proper regulation of these processes [50, 51].

Vascular remodeling to adapt to changes in tissue demand requires inflammatory activation of the endothelium and recruitment of leukocytes, mainly monocytes, which aid in remodeling [6, 7]. These processes also involve degradation of basement membranes and synthesis of a provisional, fibronectin-rich ECM. Once morphogenesis is completed, new basement membrane synthesis is a key part of the resolution phase for formation of stable, quiescent vessels [52, 53]. Atherosclerosis may be considered a form of pathological flow-dependent remodeling where ECs in regions of disturbed flow undergo inflammatory activation but can never adapt to restore quiescence [54]. WT mice show chronic inflammatory activation of the endothelium in regions of disturbed flow [55] which, when other risk factors are present, progresses to atherosclerosis. FN deposition beneath the endothelium is an early event in this process, appearing first in the regions of low grade inflammation in WT mice and increasing in atherosclerosis [13]. FN in the endothelial layer is also abundant in lesions from human arteries [56]. Moreover, several genetic manipulations that reduce FN in the vessel wall reduce atherosclerosis in mice [14-16], as does an antagonist of integrin $\alpha 5\beta 1$ [24]. Interestingly, while classic genetic studies that searched for single genes that affect artery disease identified mainly lipid metabolism and inflammatory genes, a recent analysis of gene networks identified ECM and ECM remodeling gene networks as equivalently important [57]. Thus, genetic analysis support a role for tight integration of inflammatory and ECM pathways in vascular remodeling.

Previous work showed that in cells on collagen or basement membrane, flow-induced activation of the cAMP/PKA pathway inhibits inflammatory activation of the endothelium [22]. Recent work has also identified PKA-independent anti-inflammatory actions of cAMP on inflammasome assembly[58-60]. The provisional FN-rich ECM relieves this inhibition and allows inflammatory activation. Our data show that these effects are mediated through direct binding of PDE4D5 to the integrin α5 tail. This interaction localizes PDE4D5 to focal adhesions, induces its proximity to PP2A, with subsequent dephosphorylation on an inhibitory site. This dephosphorylation increases enzymatic activity to decrease cAMP levels and increase endothelial inflammatory activation. These effects were observed both *in vitro* and *in vivo*, the latter in mice where the integrin α5 cytoplasmic domain was replaced with that of α2, and after knockdown of PDE4D5.

S651 of PDE4D5 is potentially phosphorylated by Erk2 [45]. However, in cells on collagen or basement membrane, S651 phosphorylation was high in both high and low serum, and was unaffected by the MEK inhibitor U0126 despite large changes in Erk activity, and was adhesion-independent. Instead, PDE4D5 S561 phosphorylation was controlled by matrix-specific, PP2A-dependent dephosphorylation. Thus, plating cells on FN or shear stress-dependent integrin activation results in recruitment of PDE4D5 into focal adhesions and dephosphorylation of S651.

A number of anti-inflammation drugs are in development or clinical trial for treatment of atherosclerosis [61]. Interestingly, both genetic deletion of plasma FN and an integrin $\alpha5\beta1$ antagonist reduced atherosclerotic plaque in mouse models [16 23]. However, FN contributes to hemostasis, fibrosis and other essential functions, thus, its systemic inhibition is unlikely to be clinically viable [62, 63]. The integrin α5-PDE4D interaction may therefore provide a more specific target to inhibit plaque progression without globally affecting FN function. It should also bypass adverse effects of PDE4 catalytic inhibitors [35]. Further studies will be required to understand how the molecular events and interactions defined here play out during the complex physiology

and pathology of vessel remodeling, atherosclerosis and other instances of chronic inflammation.

Methods

Cell culture

BAECs were grown in DMEM containing 10% FBS and penicillin/streptomycin. HUVECs were grown in DMEM/F12, 10% FBS, 5 mg/ml ECGS, 100 μg/ml heparin, penicillin/streptomycin or EGM media (Lonza). Mouse endothelial cells were grown in DMEM containing 20% FBS, 1X non essential amino acids (Gibco), 2 mM L-glutamate, 50 μg/ml gentamycin, 4 μg/ml amphotericine B, 100 μg/ml heparin, 5 mg/ml ECGS and penicillin/streptomycin. Primary mouse endothelial cells were isolated from the lung, using rat anti-mouse CD31 antibody (clone MEC13.3, Pharmingen, #553370) and Dynabeads (cat. no. 110.35, Invitrogen) as previously described [64]. No cell lines were used in this study.

Generation of BAECs expressing the integrin α5/2 chimera

BAECs were infected with retrovirus containing human wild type integrin α5 or the α5/2 chimera. Infected cells were selected with puromycin (0.5 μg/ml) and FACS-sorted for high expressors with mAb16 which recognizes human specific integrin α5 extracellular domain. Similar surface expression of wild type and integrin chimera was achieved by sorting.

Generation of iMAECs expressing NFκB reporter

iMAECs were first infected with lenti-virus containing human PDE4D5-GFP and sorted for the cells with similar level of expression to endogenous PDE4D5. The cells were then infected with lenti-virus for NFκB-reporter[65], which induces expression of GFP upon NFκB activation.

Plasmids and siRNA

Human integirn α5 wild type and integrin α5/2 chimera were cloned into pLPCX (Clontech) using NotI and ClaI sites. α2 tail sequence was fused to α5 sequence in frame by PCR using primers containing α2 tail sequences. siRNA resistant PDE-4D5 wild type and mutants were first cloned into pBOB-GFP vector using XbaI and AgeI sites. Then PDE4D5-GFP fragments were PCR amplified using the primers, 5'-gcaagcttatggctcagcagacaagcccgg-3' and 5'-gaattcttacttgtacagctcgtccatgc-3', then subcloned into pLPCX vector using HindIII and EcoRI sites. For introducing silent mutations into human PDE4D5, the sequence 5'-atacaaactctgagttggccttgatgta-3' was used. PDE4D siRNA sequence used in cultured cells was 5'-AAGAACUUGCCUUGAUGUACA-3' from [66]. The siRNA for *in vivo* knock-down of PDE4D was 5'-GAACGAGAUUUGUUAAAAAdTdT-3', and the siRNA for in vivo knock-down of Luciferase was 5'-CUUACGCUGAGUACUUCGAdTdT-3' [46]. siRNAs used *in vivo* were modified to prevent immunostimulation, as previously described [46, 67]. PDE4D5 F2, F3 and F4 fragments cloned into pGEX-4T1 were previously described [66]. The other PDE4D5 fragments were PCR-amplified and cloned into pGEX-4T1 vector between EcoRI and XhoI sites. For deletion fragment analysis used in figure 5E, the following amino acid sequences of PDE4D5 were fused to GST; Δ1:123-284, Δ2: 123-272, Δ3: 123-260, Δ4: 123-248. Two siRNA sequences for bovine PP2A-Cα are 5'-CCAUGACCGAAAUGUAGUAdTdT-3' and 5'-GCAUGACUGUAGAUAAGAAdTdT-3'. FAT-PDE4D5-GFP was constructed by inserting FAT domain (cloned from HUVEC cDNA) into N-terminus of pLPCX-PDE4D5-GFP construct using Gibson assembly.

Animals

The Integrin α5/2 chimera C57BL/6 strain was generated using homologous recombination by OZgene (Austrailia). Floxed-Neo mice were crossed with CMV-Cre line (stock number 006054) to create the chimera knock-in mice. For atherosclerosis analysis, integrin chimera knock-in

mice were bred with ApoE null mice (stock number 002052). All animal experiments were performed under protocols approved by Yale University Institutional Animal Care and Use. No statistical method was used to predetermine sample size. The animal experiments were not randomized. The investigators were not blinded to allocation during experiments and outcome assessment.

Shear stress experiments

Serum-starved endothelial cells were replated on glass slides coated with the indicated proteins for 5 hr before flow application. The slides were loaded into parallel plate flow chambers. Pulsatile laminar shear of 15 ± 5 dynes/cm^2 was used to mimic flow profile in athero-resistant regions of artery. Oscillatory shear of 1 ± 5 dynes/cm^2, 1 Hz was used to mimic disturbed flow in athero-prone regions.

Measurement of prostacyclin production

To measure the stable prostacyclin metabolite 6-keto-PGF1α, HUVECs were starved overnight in 1% medium containing 1% FBS, then were plated on glass slides coated with FN or matrigel for 5 hr to form a confluent monolayer. Cells were then treated with pulsatile laminar shear (15 ± 5 dynes/cm^2) for 90 min or left untreated. The medium was centrifuged to remove detached cells and 6-keto-PGF1α assayed using the ELISA kit (Enzo life sciences) according to the manufacturer's instructions.

In vivo PDE4D knock-down

PDE4D siRNA or control luciferase siRNA were packaged into endothelial-specific nanoparticles and injected at 1 mg/kg via tail vein into WT (C57Bl6) mice. After two weeks, mouse aortas were isolated and intimal RNA was prepared as described [68]. Briefly, mice were euthanized

according to Yale Universty IACUC protocol. Aortas were isolated and flushed with 250 μL QIAzol lysis reagent by insulin syringe to elute endothelial RNA, which was purified by miRNeasy mini kit (Qiagen) and amplified using a whole transcriptome amplification kit (Qiagen) according to the manufacturer's instructions. PDE4D transcript levels were measured by qRT-PCR using amplified diluted cDNA template. After confirming the dose and time course for *in vivo* PDE4D knockdown, WT (C57Bl6) mice were injected with PDE4D or control siRNA, once a week for 3 weeks. Aortas were harvested at the end of fourth week and stained for inflammatory markers. 4 male mice (3 month old) were used for each condition.

Immunohistochemistry

Mice were euthanized according to the Yale University IACUC protocol and perfused via the left ventricle with 4% paraformaldehyde (PFA). Aortas along with carotid branches were dissected and fixed overnight in PFA. For cryosections, tissue was embedded in OCT and frozen on dry ice. Longitudinal cryosections (10-15 μm) were prepared with the cryostat. For immunostaining, cryosections were fixed in -20 °C acetone for 10 minutes. Sections were blocked in IHC Tek antibody diluent for 1 hour at RT. Primary antibodies at the indicated concentrations in IHC-Tek antibody diluent and incubated overnight at 4°C. After washing 3 times in PBS, sections were incubated with Alexa Flour 598-conjugated Donkey anti rabbit/rat secondary antibody (1:200, Invitrogen) for 1 hour at RT. After washing with PBS, sections were mounted in Vectashield with DAPI (Vector Laboratories) and images taken using a confocal microscope. 4 male mice (3 month old) were used for each condition to monitor inflammatory markers on inner curvature of aortic arch. For atherosclerosis analysis, the integrin chimera mice in ApoE null background (4 male mice with age of three months) were on high fat diet for 4 months. Aortas were opened and stained en face with Sudan IV.

Antibodies

α-p-NFκB p65 (S536): rabbit mAb (93H1), Cell Signaling (3033L), 1/1,000 for immnoblotting.

α-p-Creb (S133): rabbit mAb (87G3), Cell Signaling (9198S), 1/1,000 for immunoblotting.

α-PKAc: mouse mAb, BD Transduction Laboratories (610981), 1/1,000 for immunoblotting.

α-integrin α2: rabbit polyclonal, Millipore (AB1936), 1/1,000 for immunoblotting.

α-VCAM-1: rabbit mAb (EPR5047), Abcam (ab134047), 1/200 for immunohistochemistry.

α-ICAM-1: rat mAb (YN1/1.7.4.), BioLegend (116101), 1/200 for immunohistochemistry.

α-ICAM-1: rabbit polyclonal, Abcam (ab124759), 1/1,000 for immunoblotting.

α-NFkB-p65: rabbit polyclonal (C-20), Santa Cruz (sc-372), 1/2,000 for immunoblotting.

α-Vinculin: mouse mAb (VIN-11-5), Sigma (V4505), 1/500 for immunohistochemistry.

α-fibronectin: rabbit polyclonal, Sigma (F3648), 1/400 for immunohistochemistry.

α-p-FAK (Tyr397): rabbit polyclonal, Cell Signaling (3283S), 1/1,000 for immunoblotting.

α-FAK: rabbit polyclonal, Cell Signaling (3285S), 1/1,000 for immunoblotting.

α-PP2A, C subunit: mouse mAb (1D6), Millipore (05-421), 1/1,000 for immunoblotting.

Band intensities from immunoblotting were quantified by densitometry using imageJ software.

PKA activity assay

Active PKA was isolated by pull downs with GST-PKI and quantified as described [69]. In brief, bacterially expressed GST-PKI was immobilized on GSH-agarose beads. Cell lysates were prepared in lysis buffer containing 25 mM Tris-HCl, pH 7.4, 0.5 mM EDTA, 0.5 mM EGTA, 10 mM β-mercaptoethanol, protease inhibitor cocktail and 1 mM PMSF. After brief sonication and centrifugation, the supernatants were added with 100 μM ATP and 1 mM $MgCl_2$, then incubated with the GST-PKI beads for 20 min at 4 °C and washed three times with wash buffer (50 mM Tris, pH7.4, 100 μM ATP and 1 mM $MgCl_2$). Bound active PKA was eluted with sample buffer and immunoblotted with anti-PKA catalytic subunit antibody (BD).

Immunoprecipitation

Cells were lysed in 20 mM PIPES pH 6.8, 1% TX-100, 150 mM NaCl, 150 mM sucrose, 0.2% sodium deoxycholate, 500 μM EDTA and protease inhibitors. After incubation on ice for 15 min and centrifugation, supernatants were diluted 10X in buffer containing 20 mM PIPES pH 6.8, 1% TX-100, 150 mM NaCl, 150 mM sucrose, 2.5 mM $MgCl_2$ and 2.5 mM $MnCl_2$. Ab-conjugated protein A beads were incubated with the lysates for 2 hr at 4 °C before washing with dilution buffer.

Proteomic analysis for PDE4D5 binding proteins

FLAG-tagged PDE4D5 was stably expressed in BAECs using retroviral infection. The cells were plated on FN for 30 min and lysed for immunoprecipitaion with FLAG antibody. FLAG peptides were used to elute from immune complexes from control non-infected cells and PDE4D5 expressing cells. After SDS PAGE and silver staining, specific bands were excised and submitted to Yale Keck Biotechnology Resource Laboratory for LC-MS/MS analysis.

In vitro binding assays

For the binding assay using integrin tails on beads, 30 μg of integrin α tail proteins were incubated with 6 μl of cobalt beads (Clontech). Washed beads were incubated with 100 ng of purified PDE4D5 fragment for 1 hr in buffer containing 20 mM PIPES pH 6.8, 1% TX-100, 150 mM NaCl, 150 mM sucrose. For GST-pull down analysis for PDE4D domain mapping, 5 μg of GST fusion proteins on GSH-agarose beads were incubated with 100 ng of purified integrin α5 tail proteins in buffer containing 20 mM PIPES pH 6.8, 1% TX-100, 150 mM NaCl, 150 mM sucrose and 1 mg/ml BSA for 1 hr at 4 °C, then washed and analyzed by SDS-PAGE and Western blotting.

Cell adhesion and spreading assay

Cells were detached and replated on dishes coated with either poly-L-lysine or FN (10 μg/ml) for 15 min. Adherent cells were quantified using the acid phosphatase assay [70] and normalized to the cells attached on PLL-coated dishes for 1 hr. To assess cell spreading, cells plated for the indicated times were fixed and stained with Alexa Fluor 488-conjugated wheat germ agglutinin (invitrogen, 5 μg/ml), imaged with spinning disk confocal microscopy (Nikon) and cell areas were quantified using imageJ software.

Fibronectin fibrillogenesis assay

WT or a5/2 cells were plated on FN-coated coverslips and grown until they form monolayers. Cells were incubated with 1 % FBS containing media for three days, fixed and then stained with α-FN antibody (Sigma).

Statistics and Reproducibility

Statistics were analyzed using Student's t-test or 1-way ANOVA (multiple comparisons) in GraphPad Prism 6. Statistical significance was taken as $p<0.05$. Data are represented as means ± SEM. Pull-down and co-immunoprecipitation results were confirmed in 3 independent experiments.

Data availability

Statistics Source Data are available in Supplementary Table 1. All other data are available from the authors on reasonable request.

65. Tian, J., Alimperti, S., Lei, P. & Andreadis, S.T. Lentiviral microarrays for real-time monitoring of gene expression dynamics. *Lab on a Chip* **10**, 1967-1975 (2010).
66. Kim, H.W. *et al.* Cyclic AMP Controls mTOR through Regulation of the Dynamic Interaction between Rheb and Phosphodiesterase 4D. *Molecular and Cellular Biology* **30**, 5406-5420 (2010).
67. Love, K.T. *et al.* Lipid-like materials for low-dose, in vivo gene silencing. *Proceedings of the National Academy of Sciences* **107**, 1864-1869 (2010).

68. Nam, D. *et al. Partial carotid ligation is a model of acutely induced disturbed flow, leading to rapid endothelial dysfunction and atherosclerosis*, Vol. 297. (2009).
69. Paulucci-Holthauzen, A.A. & O'Connor, K.L. Use of pseudosubstrate affinity to measure active protein kinase A. *Analytical Biochemistry* **355**, 175-182 (2006).
70. Yang, T.-T., Sinai, P. & Kain, S.R. An Acid Phosphatase Assay for Quantifying the Growth of Adherent and Nonadherent Cells. *Analytical Biochemistry* **241**, 103-108 (1996).

Acknowledgements

We thank Dr. Kenneth Yamada (NIH, USA), David Calderwood (Yale university, USA), Hyunwook Kim (POSTECH, Korea) and Arul Jayaraman (Texas A&M University, USA) for kindly providing reagents, and Dr. John Hwa (Yale university, USA) for advice on prostacyclin experiments. Lipid analysis was done by the Yale Mouse Phenotypic Center, supported by a U24 DK059635 grant. This work was funded by a National Institutes of Health grant 5R01HL75092 to M.A.S. G.S.B. is funded by an MRC project grant (MR/J007412/1). We are grateful to Rita Webber and Nicole Copeland for maintaining mouse colonies used in this study.

Author contributions

S.Y. and M.A.S. designed the project. S.Y. performed in vitro experiments and M.B. designed and performed in vivo experiments with aid of S.Y. J.E.D. prepared and provided nanoparticles. B.G.C. contributed PDE4D5 imaging. R.T.C. performed in vitro PDE assay. R.L. and D.G.A provided advice on nanoparticle formulation. S.Y. and M.A.S. wrote the manuscript with the contribution of all the authors.

References

1. Galkina, E. & Ley, K. Immune and Inflammatory Mechanisms of Atherosclerosis. *Annual Review of Immunology* **27**, 165-197 (2009).
2. Zarins, C.K. *et al.* Carotid bifurcation atherosclerosis. Quantitative correlation of plaque localization with flow velocity profiles and wall shear stress. *Circulation Research* **53**, 502-514 (1983).
3. Caro, C.G., Fitz-Gerald, J.M. & Schroter, R.C. Arterial Wall Shear and Distribution of Early Atheroma in Man. *Nature* **223**, 1159-1161 (1969).
4. Libby, P., Ridker, P.M. & Hansson, G.K. Progress and challenges in translating the biology of atherosclerosis. *Nature* **473**, 317-325 (2011).
5. Conway, D.E. & Schwartz, M.A. Flow-dependent cellular mechanotransduction in atherosclerosis. *Journal of Cell Science* **126**, 5101-5109 (2013).
6. Gaudet, A.D. & Popovich, P.G. Extracellular matrix regulation of inflammation in the healthy and injured spinal cord. *Experimental Neurology* **258**, 24-34 (2014).
7. Bollyky, P., Bogdani, M., Bollyky, J., Hull, R. & Wight, T. The Role of Hyaluronan and the Extracellular Matrix in Islet Inflammation and Immune Regulation. *Current Diabetes Reports* **12**, 471-480 (2012).
8. Papageorgiou, A.-P. & Heymans, S. Interactions between the extracellular matrix and inflammation during viral myocarditis. *Immunobiology* **217**, 503-510 (2012).
9. Grant, D.S., Kleinman, H.K. & Martin, G.R. The Role of Basement Membranes in Vascular Development. *Annals of the New York Academy of Sciences* **588**, 61-72 (1990).
10. Kim, S., Bell, K., Mousa, S.A. & Varner, J.A. Regulation of Angiogenesis in Vivo by Ligation of Integrin α5β1 with the Central Cell-Binding Domain of Fibronectin. *The American journal of pathology* **156**, 1345-1362 (2000).
11. Chiang, H.-Y., Korshunov, V.A., Serour, A., Shi, F. & Sottile, J. Fibronectin Is an Important Regulator of Flow-Induced Vascular Remodeling. *Arteriosclerosis, thrombosis, and vascular biology* **29**, 1074-1079 (2009).
12. Chiu, C.-H., Chou, C.-W., Takada, S. & Liu, Y.-W. Development and Fibronectin Signaling Requirements of the Zebrafish Interrenal Vessel. *PLoS ONE* **7**, e43040 (2012).
13. Orr, A.W. *et al.* The subendothelial extracellular matrix modulates NF-kappaB activation by flow: a potential role in atherosclerosis. *J Cell Biol* **169**, 191-202 (2005).
14. Tan, M.H. *et al. Deletion of the alternatively spliced fibronectin EIIIA domain in mice reduces atherosclerosis*, Vol. 104. (2004).
15. Babaev, V.R. *et al.* Absence of regulated splicing of fibronectin EDA exon reduces atherosclerosis in mice. *Atherosclerosis* **197**, 534-540.
16. Rohwedder, I. *et al. Plasma fibronectin deficiency impedes atherosclerosis progression and fibrous cap formation*, Vol. 4. (2012).
17. Nagel, T., Resnick, N., Atkinson, W.J., Dewey Jr, C.F. & Gimbrone Jr, M.A. Shear stress selectively upregulates intercellular adhesion molecule-1 expression in cultured human vascular endothelial cells. *Journal of Clinical Investigation* **94**, 885 (1994).
18. Bao, X., Lu, C. & Frangos, J.A. Temporal Gradient in Shear But Not Steady Shear Stress Induces PDGF-A and MCP-1 Expression in Endothelial Cells: Role of NO, NFκB, and egr-1. *Arteriosclerosis, thrombosis, and vascular biology* **19**, 996-1003 (1999).
19. Orr, A.W. *et al.* Matrix-specific p21-activated kinase activation regulates vascular permeability in atherogenesis. *The Journal of Cell Biology* **176**, 719-727 (2007).
20. Orr, A.W., Hahn, C., Blackman, B.R. & Schwartz, M.A. p21-Activated Kinase Signaling Regulates Oxidant-Dependent NF-κB Activation by Flow. *Circulation Research* **103**, 671-679 (2008).

21. Hahn, C., Orr, A.W., Sanders, J.M., Jhaveri, K.A. & Schwartz, M.A. The Subendothelial Extracellular Matrix Modulates JNK Activation by Flow. *Circulation Research* **104**, 995-1003 (2009).
22. Funk, S.D. *et al.* Matrix-Specific Protein Kinase A Signaling Regulates p21-Activated Kinase Activation by Flow in Endothelial Cells. *Circulation Research* **106**, 1394-1403 (2010).
23. Yurdagul, A. *et al.* Altered nitric oxide production mediates matrix-specific PAK2 and NF-κB activation by flow. *Molecular Biology of the Cell* **24**, 398-408 (2013).
24. Yurdagul, A. *et al.* α5β1 Integrin Signaling Mediates Oxidized Low-Density Lipoprotein–Induced Inflammation and Early Atherosclerosis. *Arteriosclerosis, thrombosis, and vascular biology* **34**, 1362-1373 (2014).
25. Orr, A.W., Ginsberg, M.H., Shattil, S.J., Deckmyn, H. & Schwartz, M.A. Matrix-specific Suppression of Integrin Activation in Shear Stress Signaling. *Molecular Biology of the Cell* **17**, 4686-4697 (2006).
26. Madamanchi, A., Santoro, S.A. & Zutter, M.M. α2β1 Integrin, in *I Domain Integrins*. (ed. D. Gullberg) 41-60 (Springer Netherlands, Dordrecht; 2014).
27. Wang, C., Baker, B.M., Chen, C.S. & Schwartz, M.A. Endothelial Cell Sensing of Flow Direction. *Arteriosclerosis, thrombosis, and vascular biology* **33**, 2130-2136 (2013).
28. Khachigian, L.M., Resnick, N., Gimbrone, M.A., Jr. & Collins, T. Nuclear factor-kappa B interacts functionally with the platelet-derived growth factor B-chain shear-stress response element in vascular endothelial cells exposed to fluid shear stress. *The Journal of Clinical Investigation* **96**, 1169-1175 (1995).
29. Glagov, S., Zarins, C., Giddens, D. & Ku, D.N. Hemodynamics and atherosclerosis. Insights and perspectives gained from studies of human arteries. *Archives of pathology & laboratory medicine* **112**, 1018-1031 (1988).
30. Frangos, S.G., Gahtan, V. & Sumpio, B. Localization of atherosclerosis: role of hemodynamics. *Archives of Surgery* **134**, 1142-1149 (1999).
31. Frangos, J.A., Eskin, S.G., McIntire, L.V. & Ives, C.L. Flow effects on prostacyclin production by cultured human endothelial cells. *Science* **227**, 1477-1479 (1985).
32. Fetalvero, K.M., Martin, K.A. & Hwa, J. Cardioprotective prostacyclin signaling in vascular smooth muscle. *Prostaglandins & Other Lipid Mediators* **82**, 109-118 (2007).
33. Stitham, J., Midgett, C., Martin, K. & Hwa, J. Prostacyclin: An inflammatory paradox. *Frontiers in Pharmacology* **2** (2011).
34. Tsai, M.-C. *et al.* Shear Stress Induces Synthetic-to-Contractile Phenotypic Modulation in Smooth Muscle Cells via Peroxisome Proliferator-Activated Receptor α/δ Activations by Prostacyclin Released by Sheared Endothelial Cells. *Circulation Research* **105**, 471-480 (2009).
35. Maurice, D.H. *et al.* Advances in targeting cyclic nucleotide phosphodiesterases. *Nat Rev Drug Discov* **13**, 290-314 (2014).
36. Baillie, G.S. Compartmentalized signalling: spatial regulation of cAMP by the action of compartmentalized phosphodiesterases. *FEBS Journal* **276**, 1790-1799 (2009).
37. Muzaffar, S., Jeremy, J.Y., Angelini, G.D. & Shukla, N. NADPH oxidase 4 mediates upregulation of type 4 phosphodiesterases in human endothelial cells. *Journal of Cellular Physiology* **227**, 1941-1950 (2012).
38. Wang, J., Bingaman, S. & Huxley, V.H. *Intrinsic sex-specific differences in microvascular endothelial cell phosphodiesterases*, Vol. 298. (2010).
39. Netherton, S.J. & Maurice, D.H. Vascular Endothelial Cell Cyclic Nucleotide Phosphodiesterases and Regulated Cell Migration: Implications in Angiogenesis. *Molecular Pharmacology* **67**, 263-272 (2005).

40. Thompson, W.J. *et al.* Regulation of cyclic AMP in rat pulmonary microvascular endothelial cells by rolipram-sensitive cyclic AMP phosphodiesterase (PDE4). *Biochemical Pharmacology* **63**, 797-807 (2002).
41. McCormick, K. & Baillie, G.S. Compartmentalisation of second messenger signalling pathways. *Current Opinion in Genetics & Development* **27**, 20-25 (2014).
42. Pullamsetti, S.S. *et al.* cAMP Phosphodiesterase Inhibitors Increases Nitric Oxide Production by Modulating Dimethylarginine Dimethylaminohydrolases. *Circulation* **123**, 1194-1204 (2011).
43. Hildebrand, J.D., Schaller, M.D. & Parsons, J.T. Identification of sequences required for the efficient localization of the focal adhesion kinase, pp125FAK, to cellular focal adhesions. *The Journal of Cell Biology* **123**, 993-1005 (1993).
44. Pfaff, M., Liu, S., Erle, D.J. & Ginsberg, M.H. Integrin β Cytoplasmic Domains Differentially Bind to Cytoskeletal Proteins. *Journal of Biological Chemistry* **273**, 6104-6109 (1998).
45. MacKenzie, S.J., Baillie, G.S., McPhee, I., Bolger, G.B. & Houslay, M.D. ERK2 Mitogen-activated Protein Kinase Binding, Phosphorylation, and Regulation of the PDE4D cAMP-specific Phosphodiesterases: THE INVOLVEMENT OF COOH-TERMINAL DOCKING SITES AND NH2-TERMINAL UCR REGIONS. *Journal of Biological Chemistry* **275**, 16609-16617 (2000).
46. Dahlman, J.E. *et al.* In vivo endothelial siRNA delivery using polymeric nanoparticles with low molecular weight. *Nat Nano* **9**, 648-655 (2014).
47. Plump, A.S. *et al.* Severe hypercholesterolemia and atherosclerosis in apolipoprotein E-deficient mice created by homologous recombination in ES cells. *Cell* **71**, 343-353 (1992).
48. Smith, J.A. Neutrophils, host defense, and inflammation: a double-edged sword. *Journal of Leukocyte Biology* **56**, 672-686 (1994).
49. Morganti-Kossmann, M.C., Rancan, M., Stahel, P.F. & Kossmann, T. Inflammatory response in acute traumatic brain injury: a double-edged sword. *Current Opinion in Critical Care* **8**, 101-105 (2002).
50. Arroyo, A.G. & Iruela-Arispe, M.L. *Extracellular matrix, inflammation, and the angiogenic response*, Vol. 86. (2010).
51. Sorokin, L. The impact of the extracellular matrix on inflammation. *Nat Rev Immunol* **10**, 712-723 (2010).
52. Stratman, A.N., Malotte, K.M., Mahan, R.D., Davis, M.J. & Davis, G.E. *Pericyte recruitment during vasculogenic tube assembly stimulates endothelial basement membrane matrix formation*, Vol. 114. (2009).
53. Davis, G.E. & Senger, D.R. Endothelial Extracellular Matrix: Biosynthesis, Remodeling, and Functions During Vascular Morphogenesis and Neovessel Stabilization. *Circulation Research* **97**, 1093-1107 (2005).
54. Hahn, C. & Schwartz, M.A. The Role of Cellular Adaptation to Mechanical Forces in Atherosclerosis. *Arteriosclerosis, thrombosis, and vascular biology* **28**, 2101-2107 (2008).
55. Jongstra-Bilen, J. *et al.* Low-grade chronic inflammation in regions of the normal mouse arterial intima predisposed to atherosclerosis. *The Journal of Experimental Medicine* **203**, 2073-2083 (2006).
56. Kakolyris, S., Karakitsos, P., Tzardi, M. & Agapitos, E. Immunohistochemical detection of fibronectin in early and advanced atherosclerosis. *In vivo (Athens, Greece)* **9**, 35-40 (1995).
57. Ghosh, S. *et al.* Systems Genetics Analysis of Genome-Wide Association Study Reveals Novel Associations Between Key Biological Processes and Coronary Artery Disease. *Arteriosclerosis, thrombosis, and vascular biology* **35**, 1712-1722 (2015).

58. Lee, G.-S. *et al.* The calcium-sensing receptor regulates the NLRP3 inflammasome through Ca2+ and cAMP. *Nature* **492**, 123-127 (2012).
59. Sokolowska, M. *et al.* Prostaglandin E2 Inhibits NLRP3 Inflammasome Activation through EP4 Receptor and Intracellular Cyclic AMP in Human Macrophages. *The Journal of Immunology* **194**, 5472-5487 (2015).
60. Yan, Y. *et al.* Dopamine Controls Systemic Inflammation through Inhibition of NLRP3 Inflammasome. *Cell* **160**, 62-73 (2015).
61. Libby, P., Okamoto, Y., Rocha, V.Z. & Folco, E. Inflammation in AtherosclerosisTransition From Theory to Practice. *Circulation Journal* **74**, 213-220 (2010).
62. Ni, H. *et al.* Plasma fibronectin promotes thrombus growth and stability in injured arterioles. *Proceedings of the National Academy of Sciences of the United States of America* **100**, 2415-2419 (2003).
63. Sakai, T. *et al.* Plasma fibronectin supports neuronal survival and reduces brain injury following transient focal cerebral ischemia but is not essential for skin-wound healing and hemostasis. *Nature medicine* **7**, 324-330 (2001).
64. Allport, J.R. *et al.* Neutrophils from MMP-9- or neutrophil elastase-deficient mice show no defect in transendothelial migration under flow in vitro. *Journal of Leukocyte Biology* **71**, 821-828 (2002).

Figure legends

Figure 1. Integrin α subunit cytoplasmic tails determine ECM-specific inflammatory signaling.

(a) Alignment of integrin α subunit tail sequences and schematic representation of integrin α5/2 chimera**. (b, c)** NFκB activation by flow. Wild type α5 or α5/2 cells on fibronectin (20 μg/ml) were subjected to 30 min laminar shear (b) or 18h oscillatory shear (c). NFκB activation was then assayed by Western blotting for S536 p65 phosphorylation (b**;** n=3, c**;** n=4). LS; Laminar shear, OS; Oscillatory shear**. (d)** Induction of ICAM-1 after 18 hr of oscillatory flow in cells expressing WT α5 vs. the α5/2 chimera on fibronectin (n=3). **(e-g)** NFκB activation by soluble atherogenic factors. Wild type BAECs on FN or diluted matrigel were stimulated with IL-1β or oxidized LDL for 30 min. NF-κB was assayed by Western blotting for pS536 p65 (e). Quantification in f (n=7) and g (n=4) shows activation relative to control cells on FN without flow. **(h)** Effect of the chimera on PKA activation. Wild type α5 or α5/2 chimera cells on FN were sheared for 15 min and active PKA was pulled down from cell lysates with GST-PKI followed by immunoblotting. Forskolin (FSK) was used as a positive control for PKA activation (n=4-8). **(i)** PKA inhibition rescues NFκB activation in α5/2 chimera cells. Chimera cells on FN were treated with the PKI 14-22 amide inhibitor or DMSO only, then subjected to oscillatory shear for 18 hr. Activation of NFκB was assayed by Western blotting (n=4). Data are represented as means ± SEM. *p<0.05 by one way ANOVA (b, c, h, i) or two-tailed t-test (d, f, g). In all panels n values represent independent experiments. Source data are provided in Supplementary Table 1. Unprocessed scans of blots are shown in Supplementary Figure 6.

Figure 2. Integrin chimera knock-in mouse showed reduced inflammation in artery

(a) Targeting strategy. These floxed, knock in mice were then bred with CMV-Cre TG mice to obtain germline replacement of the exon containing the integrin α5 cytoplasmic domain with the

integrin α2 cytoplasmic domain. **(b)** A genomic DNA fragment from homozygous knock in mice containing the integrin α5 tail was PCR-amplified and sequenced. **(c)** Validation of integrin chimera knock-in mouse. Lung homogenates from wild type and chimera knock-in mice were Western blotted with the indicated antibodies. **(d, e)** Endothelial cells isolated from adult wild type or chimera knock-in homozygous mice were replated on dishes coated with poly-L-lysine or FN (10 μg/ml). **(d)** After 15 min, adherent cells were quantified using the acid phosphatase assay and normalized to the cells attached on PLL (n=3 independent experiments). Error bars are SEM. **(e)** Cell spreading at the indicated times was determined as described in Methods. For each condition, n=20 images (~10 cells/field) pooled across three independent experiments. The box plot shows the median, with upper and lower percentiles, and the bars show maxima and minima values. Source data for d are available in Supplementary Table 1. **(f)** Inflammatory markers in an athero-prone artery segment of knock-in mice. Aortas from wild type and chimera knock-in homozygous mice were stained for the indicated proteins and the lesser curvature of the arch was examined. Staining intensity was quantified as described in Methods (n=5 mice for each type). L; Lumen. Data are represented as means ± SEM. *p<0.05 by two-tailed t-test. Scale bar: 35 μm. Quantification data from individual mice are provided in Supplementary Table 1.

Figure 3. Prostacyclin mediates shear-dependent PKA activation but is ECM-independent

(a) HUVECs on matrigel were pretreated with aspirin (ASA, COX inhibitor, 10 μM) or prostacyclin receptor antagonist (RO1138452, 100 nM) then sheared for 15 min. PKA activity was measured as in Fig. 1 (n=3). LS; Laminar shear, OS: Oscillatory shear. **(b, c)** HUVECs on matrigel pretreated with aspirin (10 μM) or RO1138452 (100 nM) were exposed to oscillatory shear for 18 hr, then NFκB S536 phosphorylation measured by Western blotting. (b; n=4, c; n=3). **(d)** α5/2 chimera expressing BAECs on FN were treated with indometacin (10 μM) or

RO1138452 (100 nM), then sheared for 15 min. PKA activity was measured as in a (n=3). **(e, f)** α5/2 chimera cells on FN pretreated with indometacin (10 μM) or RO1138452 (100 nM), were exposed to oscillatory shear for 18 hr. NFκB activation was measured as in **b** and **c** (n=5). **(g)** HUVECs on matrigel or FN were subjected to pulsatile shear (15 dynes/cm2±5 dynes/cm^2) for 90 min. 6-keto-PGFα in the medium was measured by ELISA (n=4). Data are represented as means ± SEM. *p<0.05 by one way ANOVA (b, c, e, f) or two-tailed t-test (a, d, g). In all panels n values represent independent experiments. Source data are provided in Supplementary Table 1.

Figure 4. Involvement of PDE4D in ECM-dependent inflammatory signaling

(a) BAECs on FN were treated with the PDE4 inhibitor rolipram (1 μM), sheared, and PKA activity assayed as in Fig 1. (n=5). **(b)** BAECs on FN or collagen were treated with rolipram (1 μM) and assayed for NFκB as before (n=3). **(c)** HUVEC lysates were immunoprecipitated with two different PDE4D5 antibodies and Western blots probed for integrin α5 or integrin α2. Similar results were obtained in 3 experiments. **(d)** BAECs expressing wild type integrin α5 or the α5/2 chimera were immunoprecipitated with human-specific integrin α5 antibody recognizing the extracellular region. Western blots were probed for PDE4D5 and for the integrin β1 subunit. Similar results were obtained in 4 experiments. **(e)** BAECs were transfected with siRNA against PDE4D and then rescued with control or PDE4D5-GFP retrovirus. Cells were subjected to oscillatory shear and NFκB assayed as before. (n=4). **(f)** BAECs expressing wild type PDE4D5 or FAT-PDE4D5 were plated on matrigel for 5hr and subjected to oscillatory shear. NFκB S536 phosphorylation and Creb S133 phosphorylation were measured by Western blotting (n=4). Data are represented as means ± SEM. *p<0.05 by one way ANOVA (a, e, f) or two-tailed t-test (b). In all panels n values represent independent experiments. Source data are provided in Supplementary Table 1. Unprocessed scans of blots are shown in Supplementary Figure 6.

Figure 5. Mapping the integrin binding site on PDE4D5.

(a) Schematic representation of PDE4D5 and fragments used for pull-down assays. **(b)** HUVEC lysates were incubated with GST-tagged fragments of PDE4D5 and probed for integrin α5. Results are representative of 3 independent experiments. **(c)** To test whether the interaction is direct, integrin α tails immobilized on cobalt beads were incubated with purified PDE4D5-F2 fragment. Beads were washed and bound material was analyzed by western blotting. (α5R = scrambled sequence of α5 tail.) **(d)** Deletion constructs used for detailed mapping and critical residues for binding. **(e, f)** The indicated PDE4D5 fragments and mutants were immobilized on GSH beads and incubated with α5 tail protein used in **c**. Bound α5 tail protein was detected by Western blotting with integrin α5 antibody against cytoplasmic tail. Results are representative of 3 independent experiments. **(g)** BAECs expressing GFP-tagged PDE4D5 wild type or 4E mutant were plated on fibronectin or collagen and sheared for 15 min. The cells were fixed and stained for the focal adhesion marker, vinculin. Results are representative of 3 independent experiments. Scale bar: 50 μm. **(h)** BAECs stably expressing integrin α5 binding-deficient PDE4D5 mutants (4A and 4E) or catalytically inactive mutant (D556A) were transfected with siRNA to knock down the endogenous PDE4D, then were subjected to oscillatory shear for 18 hr. NFκB activity was assayed as in Fig. 1; (n=3 independent experiments). Data are represented as means ± SEM. *$p<0.05$ by two-tailed t-test. Source data are provided in Supplementary Table 1. Unprocessed scans of blots are shown in Supplementary Figure 6.

Figure 6. ECM-dependent regulation of PDE4D phosphorylation

(a) BAECs expressing wild type or 4E mutant of PDE4D5 were plated on collagen or FN for 5 hr then sheared for 15 min. Cell lysates were probed for anti-pS651-PDE4D (n=4-6). **(b)** BAECs

expressing WT integrin α5 or the α5/2 chimera on fibronectin, transfected with PDE4D5, then sheared for 15 min. S651 phosphorylation was assayed by Western blotting as in **a** (n=3). **(c)** BAECs expressing PDE4D5 wild type or the 4E mutant or chimera cells expressing PDE4D5 wild type were kept in suspension for 90 min then replated on FN-coated dishes for the indicated times. S651 phosphorylation was assayed by Western blotting (n=3). **(d, e)** BAECs in which endogenous PDE4D5 was knocked down were reconstituted with WT, phospho-deficient S651A or phospho-mimetic S651E mutants. The cells were replated on collagen (d) (n=3) or FN (e) (n=6) then subject to oscillatory shear for 2 hrs. NFκB activity was assayed as in Fig 1. In all panels n values represent independent experiments. Data are represented as means ± SEM. *p<0.05 by one way ANOVA (a, b, d) or two-tailed t-test (c, e). Source data are provided in Supplementary Table 1. Unprocessed scans of blots are shown in Supplementary Figure 6.

Figure 7. *In vivo* PDE4D knock-down reduces flow-dependent inflammation

(a) Validation of siRNA used for *in vivo* knock-down. Immortalized mouse aortic endothelial cells (iMAEC) were expressed with GFP-tagged human PDE4D5 and transfected with siRNA used for nanoparticle formulation. NFκB activation was assayed either by measuring GFP-reporter expression under control of NFκB responsive element or ICAM-1 induction. Data are represented as means ± SEM. *p<0.05 and $^{\#}$p=0.079 by two-tailed t-test. (n=3 independent experiments) Source data are provided in Supplementary Table 1. **(b)** Nano-particles containing PDE4D siRNA or luciferase siRNA (1 mg/kg) were injected intravenously. Aortas from treated mice were isolated and stained for the indicated molecules to assay inflammatory markers in lesser curvature (n=5 mice). Scale bar: 35 μm. **(c)** Integrin chimera knock-in mice were bred with ApoE null mice and fed with high fat diet for 4 months. Aortas were opened and stained en face with Sudan IV (n=4 mice). Plaque area and numbers were quantified. Data are represented

as means ± SEM. *p<0.05 by two-tailed t-test. Quantification data from individual mice are provided in Supplementary Table 1.

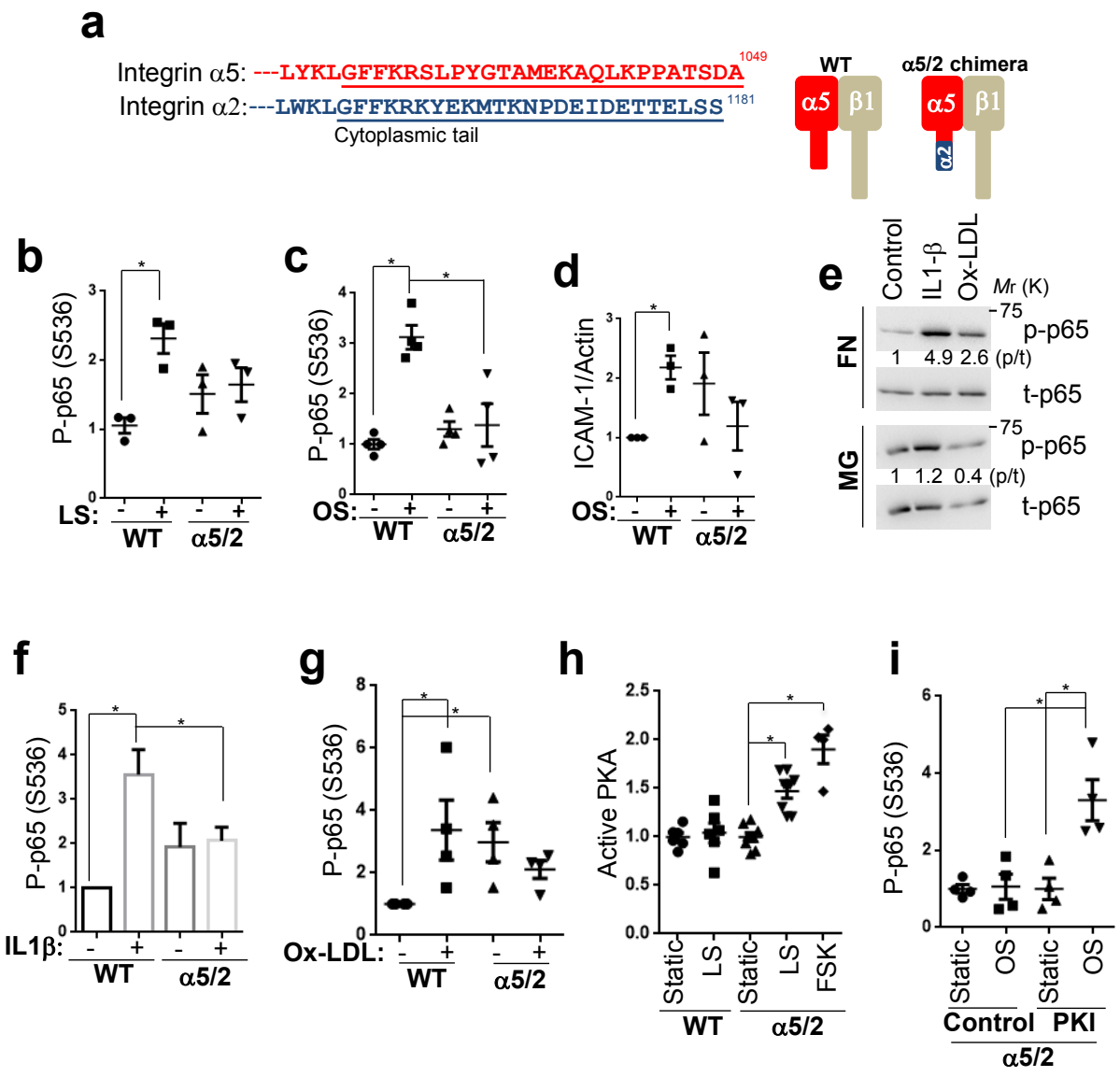
a
Integrin α5: ---LYKLGFFKRSLPYGTAMEKAQLKPPATSDA 1049
Integrin α2:---LWKLGFFKRKYEKMTKNPDEIDETTELSS 1181
Cytoplasmic tail
WT
α5/2 chimera
α5
β1
α2
b
P-p65 (S536)
LS:
WT
α5/2
c
P-p65 (S536)
OS:
WT
α5/2
d
ICAM-1/Actin
OS:
WT
α5/2
e
Control
IL1-β
Ox-LDL
Mr (K)
75
p-p65
1 4.9 2.6 (p/t)
t-p65
FN
MG
75
p-p65
1 1.2 0.4 (p/t)
t-p65
f
P-p65 (S536)
IL1β:
WT
α5/2
g
P-p65 (S536)
Ox-LDL:
WT
α5/2
h
Active PKA
Static
LS
Static
LS
FSK
WT
α5/2
i
P-p65 (S536)
Static
OS
Static
OS
Control
PKI
α5/2

Figure 1

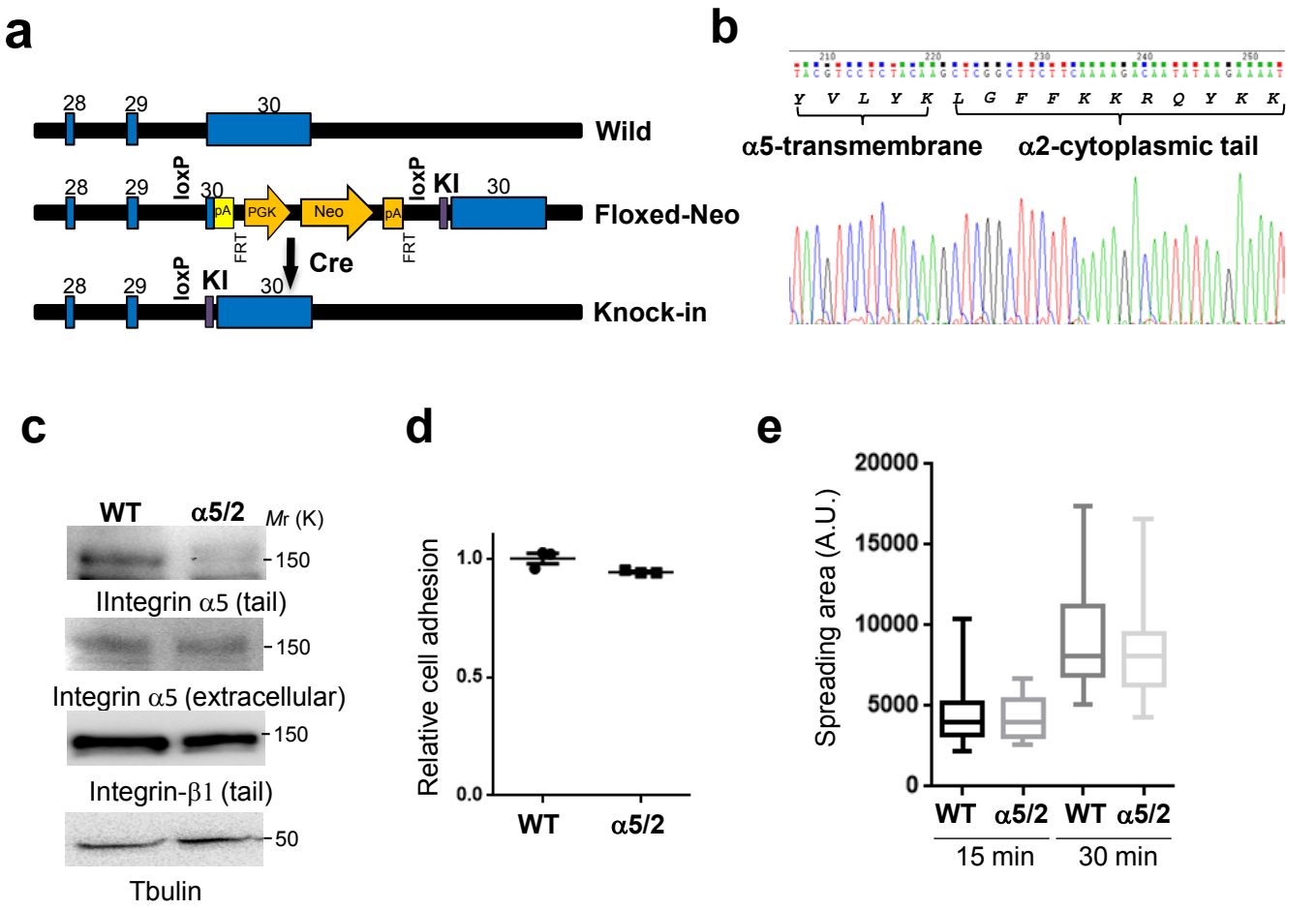
a
28
29
30
Wild
loxP
KI
pA
PGK
Neo
FRT
Floxed-Neo
Cre
Knock-in
b
Y V L Y K L G F F K K R Q Y K K
α5-transmembrane
α2-cytoplasmic tail
c
WT
α5/2
Mr (K)
150
IIntegrin α5 (tail)
Integrin α5 (extracellular)
Integrin-β1 (tail)
50
Tbulin
d
Relative cell adhesion
1.0
0.5
0.0
e
Spreading area (A.U.)
20000
15000
10000
5000
0
15 min
30 min
f
Ascending aorta
Inner curvature
Descending aorta
Fibronectin
ICAM-1
VCAM-1
L
FN staining %
ICAM-1 staining %
VCAM-1 staining %
*

Figure 2

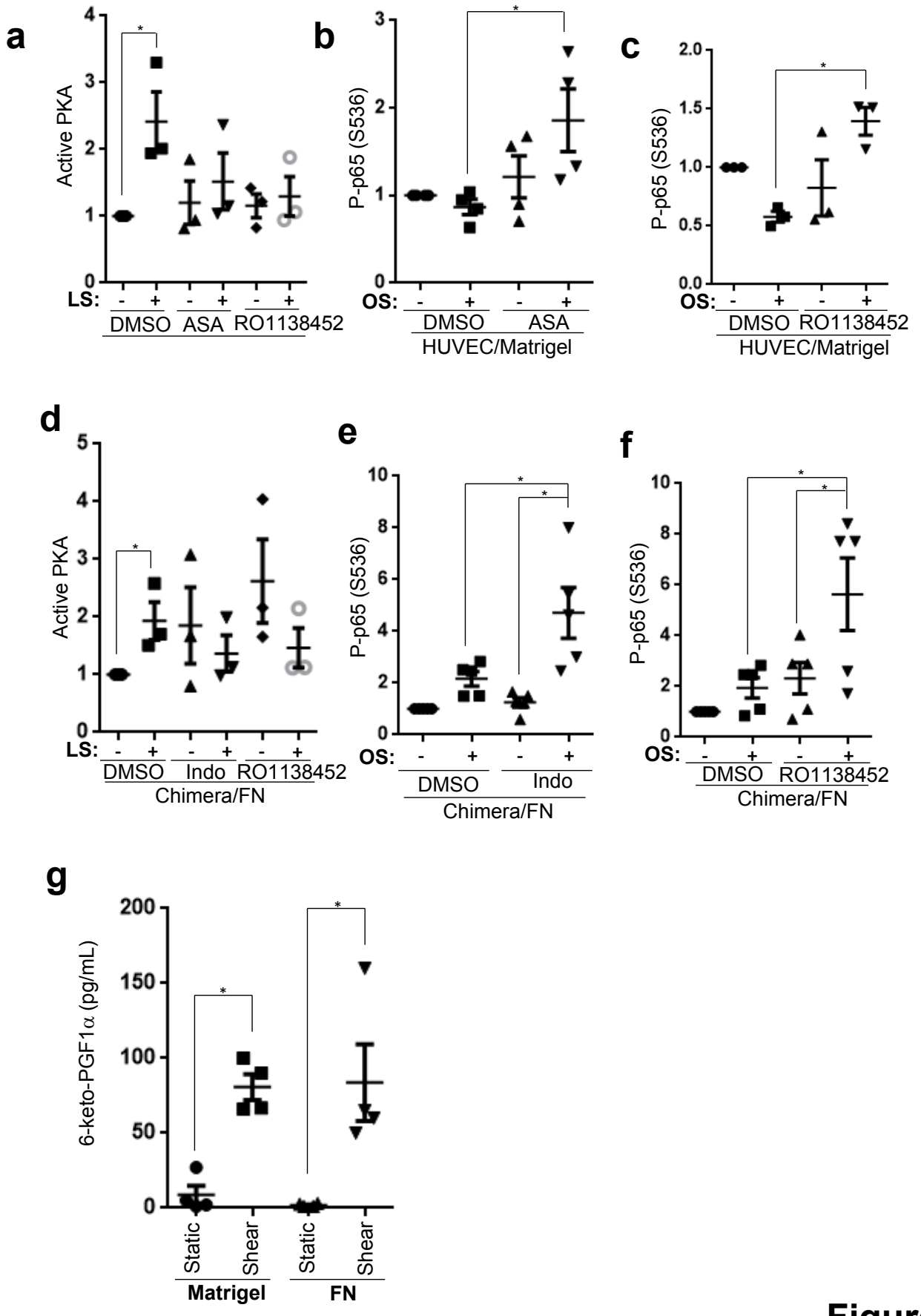
a
Active PKA
LS:
DMSO
ASA
RO1138452
b
P-p65 (S536)
OS:
DMSO
ASA
HUVEC/Matrigel
c
P-p65 (S536)
OS:
DMSO
RO1138452
HUVEC/Matrigel
d
Active PKA
LS:
DMSO
Indo
RO1138452
Chimera/FN
e
P-p65 (S536)
OS:
DMSO
Indo
Chimera/FN
f
P-p65 (S536)
OS:
DMSO
RO1138452
Chimera/FN
g
6-keto-PGF1α (pg/mL)
Static
Shear
Static
Shear
Matrigel
FN

Figure 3

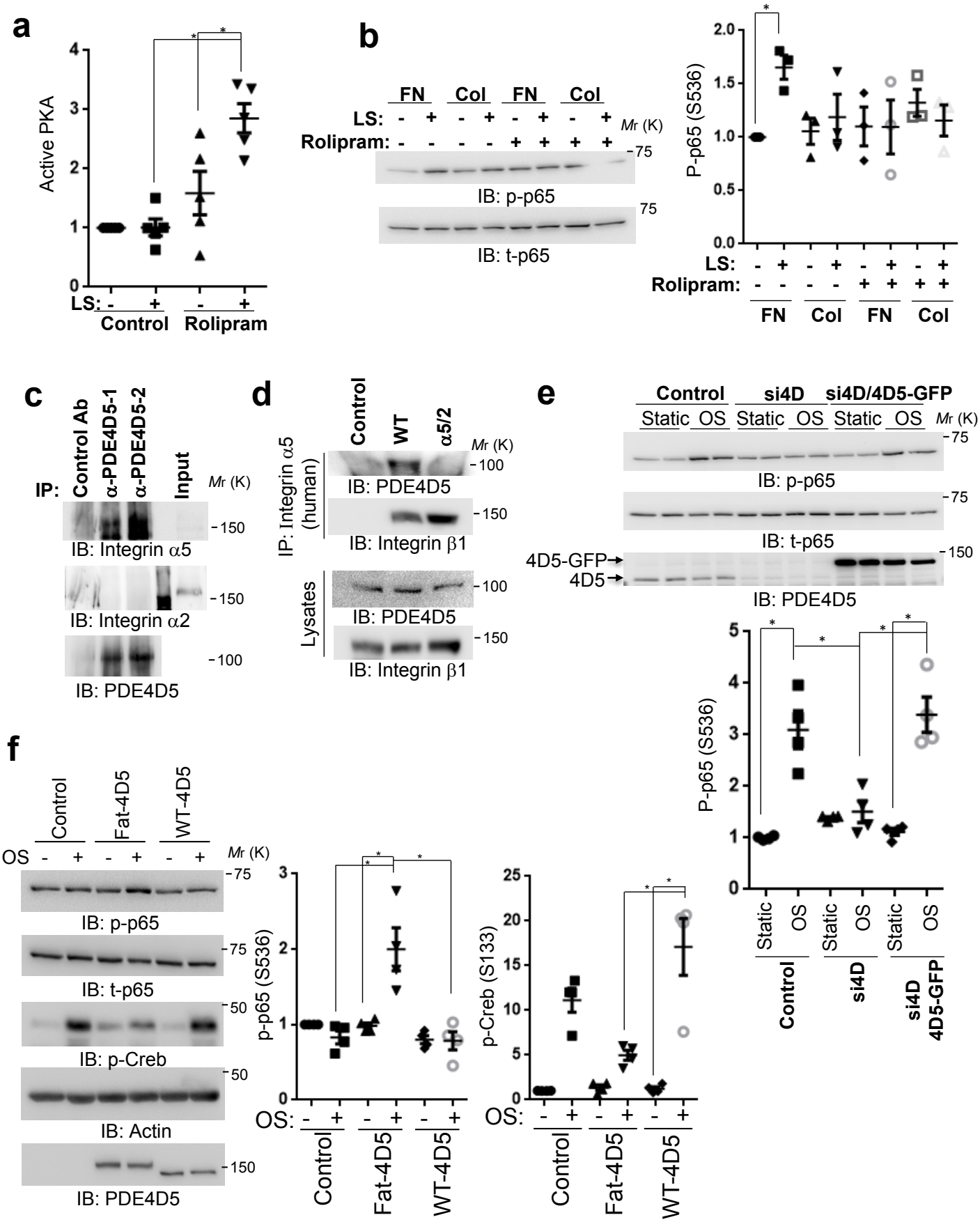
a
Active PKA
LS: - + - +
Control
Rolipram
b
FN Col FN Col
LS: - + - + - + - +
Rolipram: - - - - + + + +
Mr (K)
75
IB: p-p65
75
IB: t-p65
P-p65 (S536)
LS: - + - + - + - +
Rolipram: - - - - + + + +
FN Col FN Col
c
IP:
Control Ab
α-PDE4D5-1
α-PDE4D5-2
Input
Mr (K)
150
IB: Integrin α5
150
IB: Integrin α2
100
IB: PDE4D5
d
Control
WT
α5/2
Mr (K)
IP: Integrin α5 (human)
100
IB: PDE4D5
150
IB: Integrin β1
Lysates
100
IB: PDE4D5
150
IB: Integrin β1
e
Control
si4D
si4D/4D5-GFP
Static OS Static OS Static OS
Mr (K)
75
IB: p-p65
75
IB: t-p65
4D5-GFP
4D5
150
IB: PDE4D5
P-p65 (S536)
Static OS Static OS Static OS
Control
si4D
si4D 4D5-GFP
f
Control
Fat-4D5
WT-4D5
OS - + - + - +
Mr (K)
75
IB: p-p65
75
IB: t-p65
50
IB: p-Creb
50
IB: Actin
150
IB: PDE4D5
p-p65 (S536)
OS: - + - + - +
Control
Fat-4D5
WT-4D5
p-Creb (S133)
OS: - + - + - +
Control
Fat-4D5
WT-4D5

Figure 4

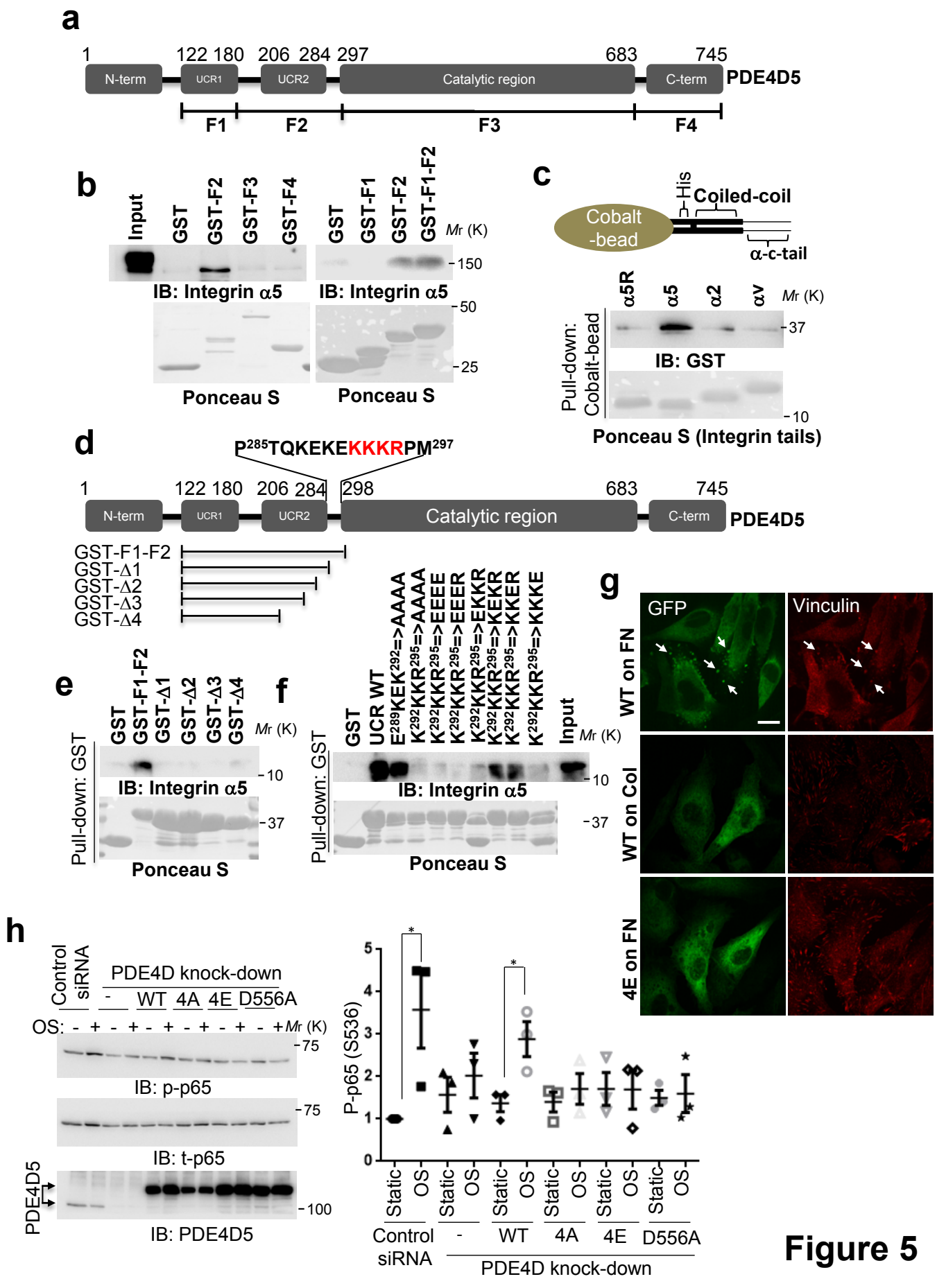
a
1
122 180
206 284 297
683
745
N-term
UCR1
UCR2
Catalytic region
C-term
PDE4D5
F1
F2
F3
F4
b
Input
GST
GST-F2
GST-F3
GST-F4
GST
GST-F1
GST-F2
GST-F1-F2
Mr (K)
150
IB: Integrin α5
IB: Integrin α5
50
25
Ponceau S
Ponceau S
c
His
Coiled-coil
Cobalt -bead
α-c-tail
α5R
α5
α2
αV
Mr (K)
Pull-down: Cobalt-bead
37
IB: GST
10
Ponceau S (Integrin tails)
d
P285TQKEKEKKKRPM297
1
122 180
206 284
298
683
745
N-term
UCR1
UCR2
Catalytic region
C-term
PDE4D5
GST-F1-F2
GST-Δ1
GST-Δ2
GST-Δ3
GST-Δ4
e
GST
GST-F1-F2
GST-Δ1
GST-Δ2
GST-Δ3
GST-Δ4
Mr (K)
Pull-down: GST
10
IB: Integrin α5
37
Ponceau S
f
GST
UCR WT
E289KEK292=>AAAA
K292KKR295=>AAAA
K292KKR295=>EEEE
K292KKR295=>EEER
K292KKR295=>EKKR
K292KKR295=>KEKR
K292KKR295=>KKER
K292KKR295=>KKKE
Input
Mr (K)
Pull-down: GST
10
IB: Integrin α5
37
Ponceau S
g
GFP
Vinculin
WT on FN
WT on Col
4E on FN
h
Control siRNA
PDE4D knock-down
-
WT
4A
4E
D556A
OS: - + - + - + - + - + - + Mr (K)
75
IB: p-p65
75
IB: t-p65
PDE4D5
100
IB: PDE4D5
P-p65 (S536)
5
4
3
2
1
0
*
*
Static
OS
Control siRNA
PDE4D knock-down
-
WT
4A
4E
D556A

Figure 5

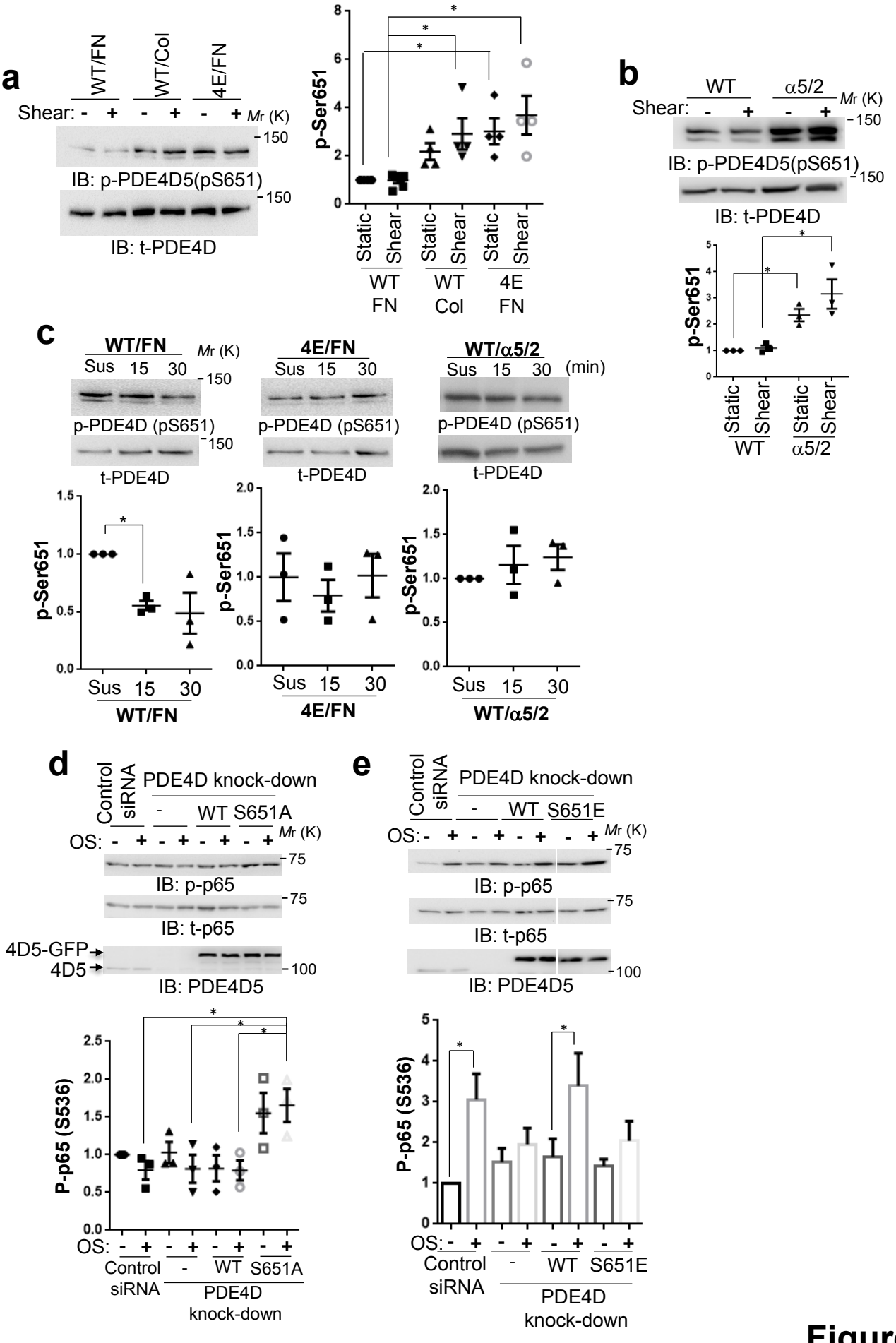
a
WT/FN
WT/Col
4E/FN
Shear: - + - + - +
Mr (K)
150
IB: p-PDE4D5(pS651)
150
IB: t-PDE4D
p-Ser651
Static
Shear
WT FN
WT Col
4E FN
b
WT
α5/2
Shear: - + - +
Mr (K)
150
IB: p-PDE4D5(pS651)
150
IB: t-PDE4D
p-Ser651
Static
Shear
WT
α5/2
c
WT/FN
4E/FN
WT/α5/2
Sus 15 30 (min)
Mr (K)
150
p-PDE4D (pS651)
150
t-PDE4D
p-Ser651
Sus 15 30
WT/FN
4E/FN
WT/α5/2
d
Control siRNA
PDE4D knock-down
- WT S651A
OS: - + - + - + - +
Mr (K)
75
IB: p-p65
75
IB: t-p65
4D5-GFP
4D5
100
IB: PDE4D5
P-p65 (S536)
OS: - + - + - + - +
Control siRNA
PDE4D knock-down
- WT S651A
e
Control siRNA
PDE4D knock-down
- WT S651E
OS: - + - + - + - +
Mr (K)
75
IB: p-p65
75
IB: t-p65
100
IB: PDE4D5
P-p65 (S536)
OS: - + - + - + - +
Control siRNA
PDE4D knock-down
- WT S651E

Figure 6

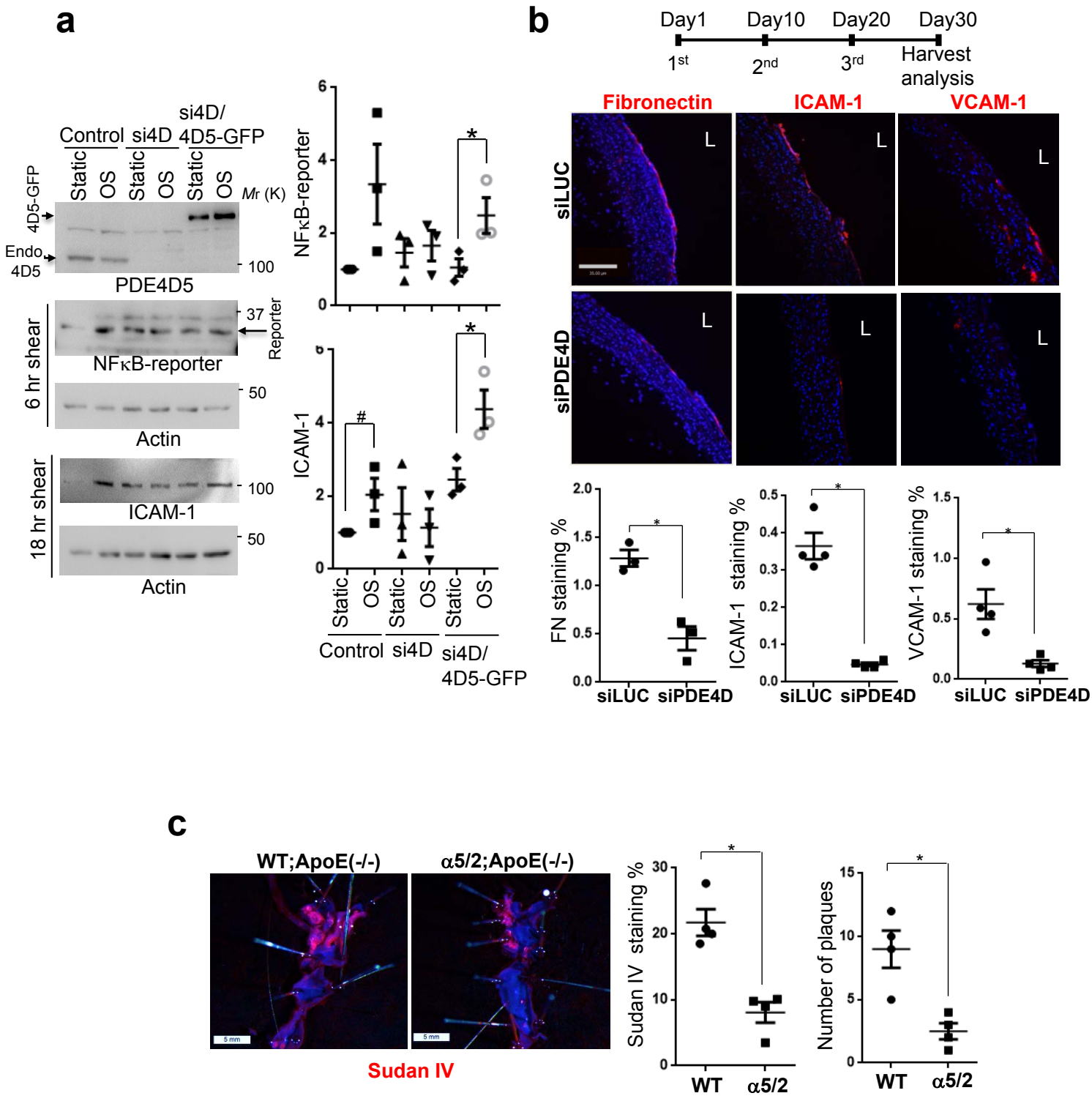
a
Control
si4D
si4D/ 4D5-GFP
Static
OS
Mr (K)
4D5-GFP
Endo 4D5
PDE4D5
100
6 hr shear
NFκB-reporter
37
Reporter
50
Actin
18 hr shear
ICAM-1
100
50
Actin
NFκB-reporter
ICAM-1
Control
si4D
si4D/ 4D5-GFP
b
Day1
Day10
Day20
Day30
1st
2nd
3rd
Harvest analysis
Fibronectin
ICAM-1
VCAM-1
siLUC
siPDE4D
L
FN staining %
ICAM-1 staining %
VCAM-1 staining %
siLUC
siPDE4D
c
WT;ApoE(-/-)
α5/2;ApoE(-/-)
Sudan IV
Sudan IV staining %
Number of plaques
WT
α5/2

Figure 7

Supplementary Figure 1. Characterization of α5/2 chimera endothelial cells

(a) BAECs expressing human integrin wild type α5 or the α5/2 chimera were stained with mAb16 that recognizes human integrin α5 extracellular domain. **(b)** Wild type α5 or the α5/2 chimera cells were lysed and immunoprecipitated with mAb16 to isolate exogenous human integrin α proteins. Western blots with antibodies against the α5 and α2 cytoplasmic tails confirm the sequences (upper and middle panels), and show similar pairing with the β1 subunit (lower panel). **(c, d)** Wild type α5 and α5/2 chimera cells spreading on fibronectin. BAECs expressing wild type integrin α5 or the chimera were detached and replated on dishes coated with fibronectin (10 μg/ml) for the indicated times. The cells were either fixed and stained with wheat germ agglutinin (c) or lysed and subjected to immunoblotting for FAK phosphorylation (Y397) (d). **(e)** Wild type α5 or α5/2 chimera cells were plated on fibronectin and grown to monolayer and then kept in low-serum media (1% FBS) for two days to induce fibronectin fibrillogenesis. The cells were fixed and stained for fibronectin. For each condition, n=30 images pooled across three independent experiments were averaged. The box plot shows the median, with upper and lower percentiles, and the bars show maxima and minima values. **(f)** Wild type α5 or α5/2 chimera cells were plated on fibronectin and sheared for 36 hrs (20dynes/cm^2). Cells were stained with phalloidin and Hoechst and alignment in the direction of flow was quantified (±30°). Scale bars: 50 μm. n=10 images (60-100 cells/field) were used for quantification for each condition. Error bars are SEM.

Supplementary Figure 2. PDE4D5 is responsible for ECM-dependent inflammation in endothelial cells.

(a) BAECs on FN or collagen were treated with rolipram (1 μM) and assayed for AMPK activation. **(b)** Immunoblotting HUVEC lysate with pan PDE4D antibody detects the major band co-migrating with reference PDE4D5 (left panel). The band was diminished by transfection with PDE4D siRNA, demonstrating specificity. Similarly, PDE4D5 was the only isoform detectable in BAEC lysate with immunobotting using pan PDE4D antibody or PDE4D5 specific antibody (right two panels). * indicates non-specific bands. **(c)** BAECs expressing wild type PDE4D5 or FAT-PDE4D5 were plated on MG for 1hr to monitor GFP signal.

Supplementary Figure 3. PP2A regulates PDE4D5 phosphorylation and inflammation

(a) Identification of PP2A as a PDE4D5 binding protein. FLAG-PDE4D5 expressing BAECs on FN were lysed and immunoprecipitated with FLAG antibody. Bound protein with size of 35 kDa was submitted for mass analysis and identified as PP2A catalytic subunit. **(b)** BAECs expressing FLAG-tagged PDE4D5 were plated on either FN or matrigel for indicated times. PDE4D5 was immunoprecipitated with FLAG antibody and eluted with FLAG peptides. Similar results were obtained in 3 experiments. **(c)** BAECs expressing PDE4D5 wild type were kept in suspension for 90 min then replated on FN-coated dishes for the indicated times. For okadaic acid treatment, cells in suspension were added with 5 nM OA for last 20 min before replating on FN. S651 phosphorylation was assayed by Western blotting (n=4 independent experiments). **(d)** BAECs expressing PDE4D5 were plated on FN for 5 hr then pretreated with DMSO or okadaic acid (OA, 5 nM) and then stimulated with IL1β for 30 min. S651 phosphorylation was assayed by Western blotting (n=3 independent experiments). **(e)** BAECs expressing PDE4D5 were transfected with a siRNAs targeting PP2A catalytic subunit. The cells were replated on FN then subject to laminar shear for 30 min. **(f)** BAECs were plated on FN for 5 hr then pretreated with DMSO or okadaic acid (OA, 5 nM) and then stimulated with IL1β for 30 min. NFκB activity was assayed by Western blotting (n=3 independent experiments). **(g)** BAECs were transfected with two different siRNAs targeting the PP2A catalytic subunit. The cells were replated on FN then subject to oscillatory shear for 2 hrs (n=3 independent experiments). Data are represented as means ± SEM. *$p<0.05$ by one way ANOVA (d, g) or two-tailed t-test (c, f). Source data are provided in Supplementary Table 1.

Supplementary Figure 4. Effect of PP2A inhibition on endothelial cell adhesion

(a) BAECs were transfected with PP2A siRNA or treated with okadaic acid (OA, 5 nM, 1hr) and plated on FN (10 μg/ml) for 1hr. Cell adhesion was quantified as described in Supplementary Fig. 2 (n=3 independent experiments) and cell morphology was examined after fixation and phalloidin and nuclear staining. Error bars are SEM. Scale bar: 100 μm. **(b)** BAECs treated as (a) were plated on FN (10 μg/ml) for indicated times and FAK phosphorylation was measured by Western blotting.

Supplementary Figure 5. *In vivo* knock-down of endothelial PDE4D

(a) NIH3T3 cells were transfected with either luciferase siRNA or mouse PDE4D siRNA used for *in vivo* knock-down. After 72h, PDE4D5 was assayed by Western blotting with tubulin as a loading control. **(b)** Nano-particles containing PDE4D siRNA or luciferase siRNA (1 mg/kg) were injected intravenously. After two weeks, mouse aortas were isolated, and endothelial expression of PDE4D was assayed by qPCR (n=4). (**c**) Serum lipid profile of α5/2; ApoE(-/-) mice after high fat diet (n=6 mice). Data are represented as means ± SEM. *p<0.05 by two-tailed t-test. Source data are provided in Supplementary Table 1.

Supplementary Figure 6. Unprocessed scans of key blots

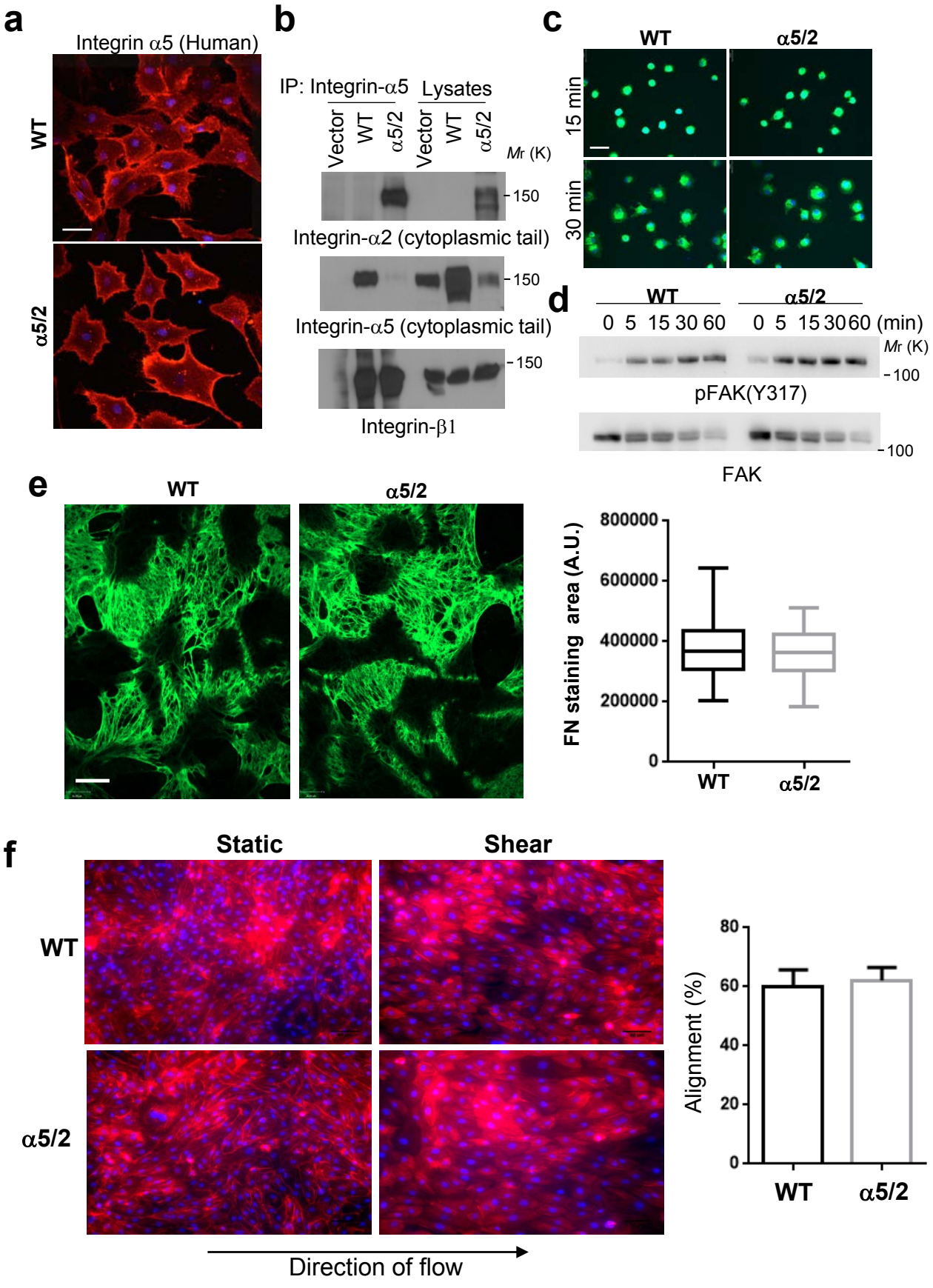

Supplementary Fig. 1

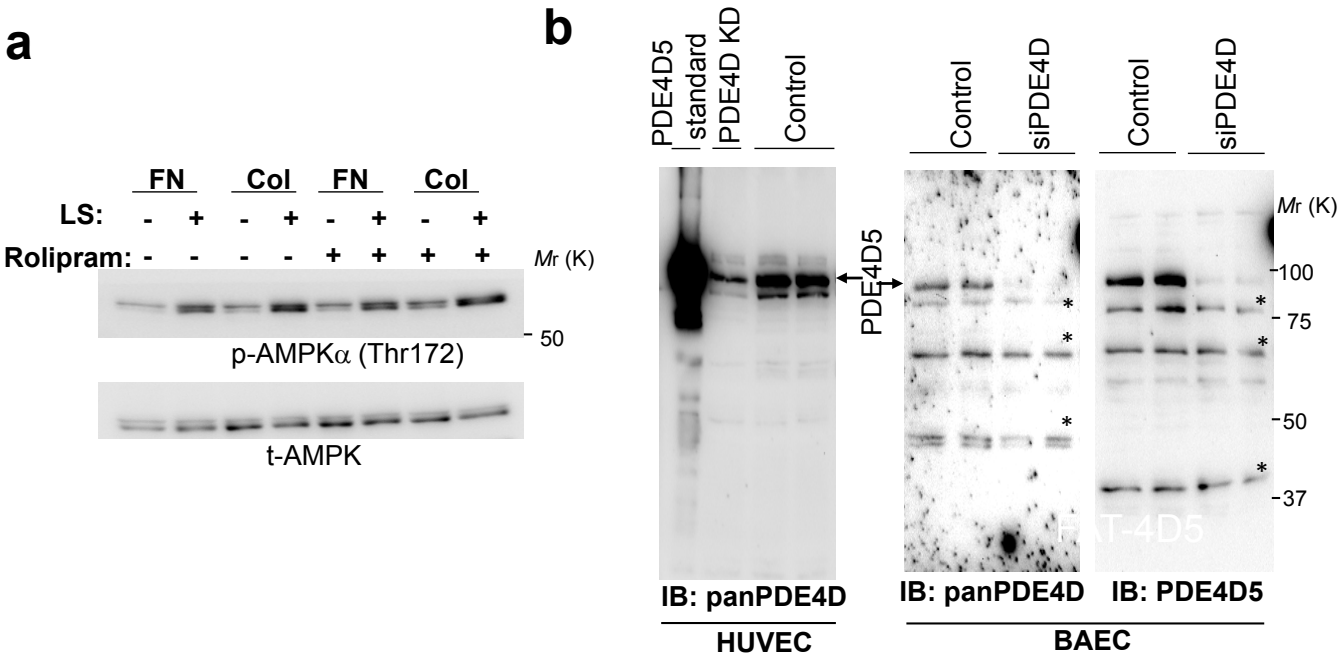

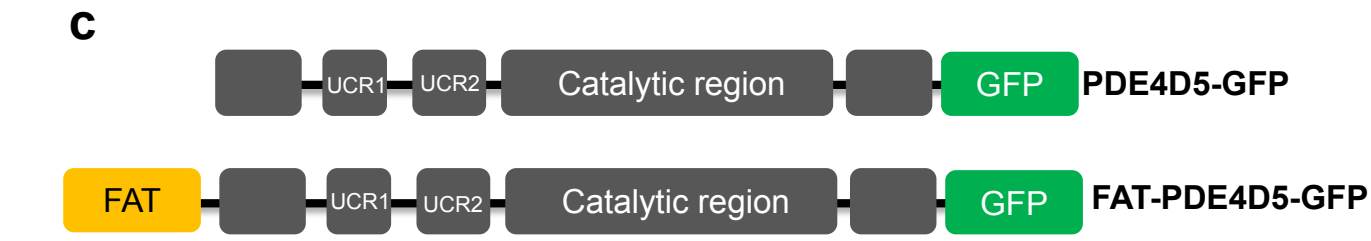

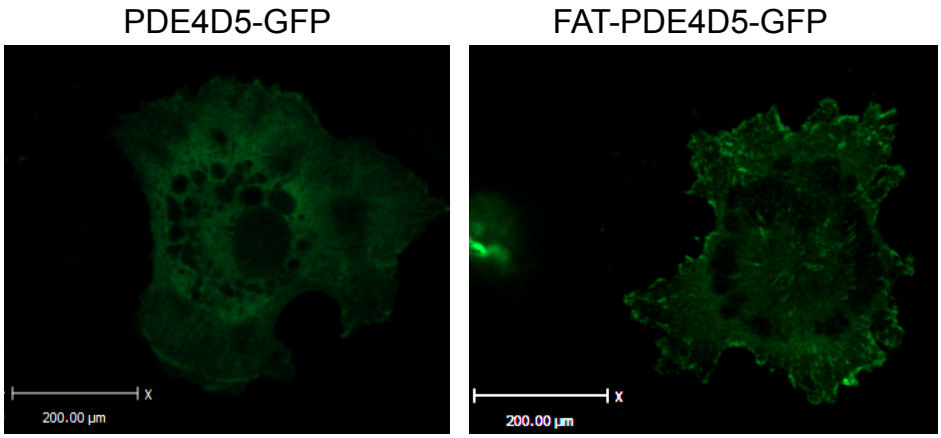

Supplementary Fig. 2

a

LCMS Peptides

Protein ID	PP2AA_BOVIN
Protein Name	Serine/threonine-protein phosphatase 2A catalytic subunit alpha isoform OS=Bos taurus GN=PPP2CA PE=1 SV=1
Percent Coverage	3.6

One peptide identified with score greater than identity score

Score	Expectation	Peptide Sequence	Start	End	M/Z	Ion Mass	Ion Mass(calc)	Delta	ppm	Charge
73.48	0.0000016	K.YSFLQFDPAPR.R	284	294	670.8371	1339.6597	1339.6561	0.0036	2.7	2

mdekvftkeldqwieqlneckqlsesqvkslcekakeiltkesnvqevrcpvtvcgdvhgqfhdlmelfriggkspdtnylfmgdyvdrgyysvet
vtllvalkvryreritilrgnhesrqitqvygfydeclrkygnanvwkyftdlfdylpltalvdgqifclhgglspsidtldhiraldrlqevphegpmcdllws
dpddrggwgisprgagytfgqdisetfnhangltlvsrahqlvmegynwchdrnvvtifsapnycyrcgnqaaimelddtlkysflqfdpaprrgep
hvtrrtpdyfl

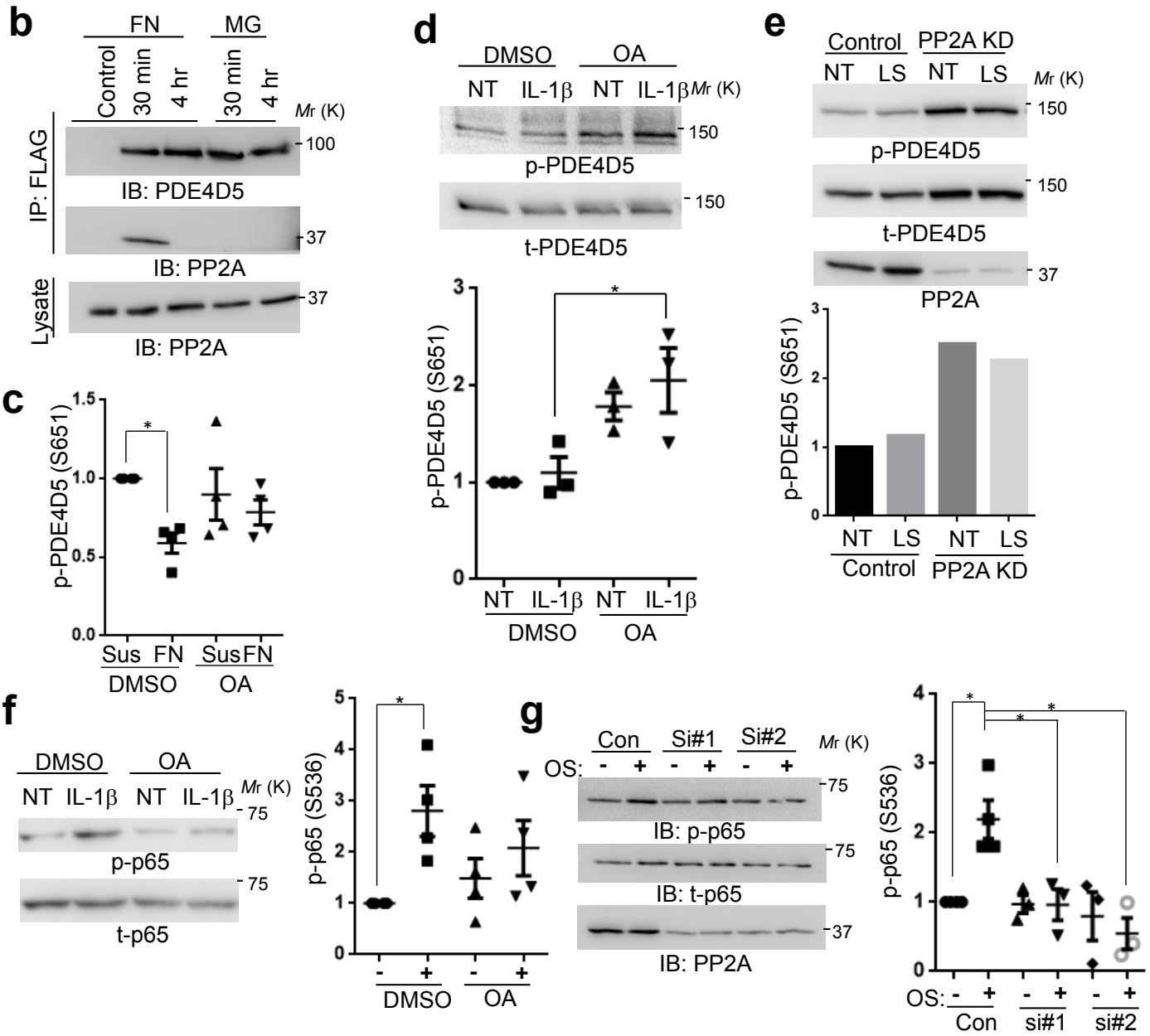

Supplementary Fig. 3

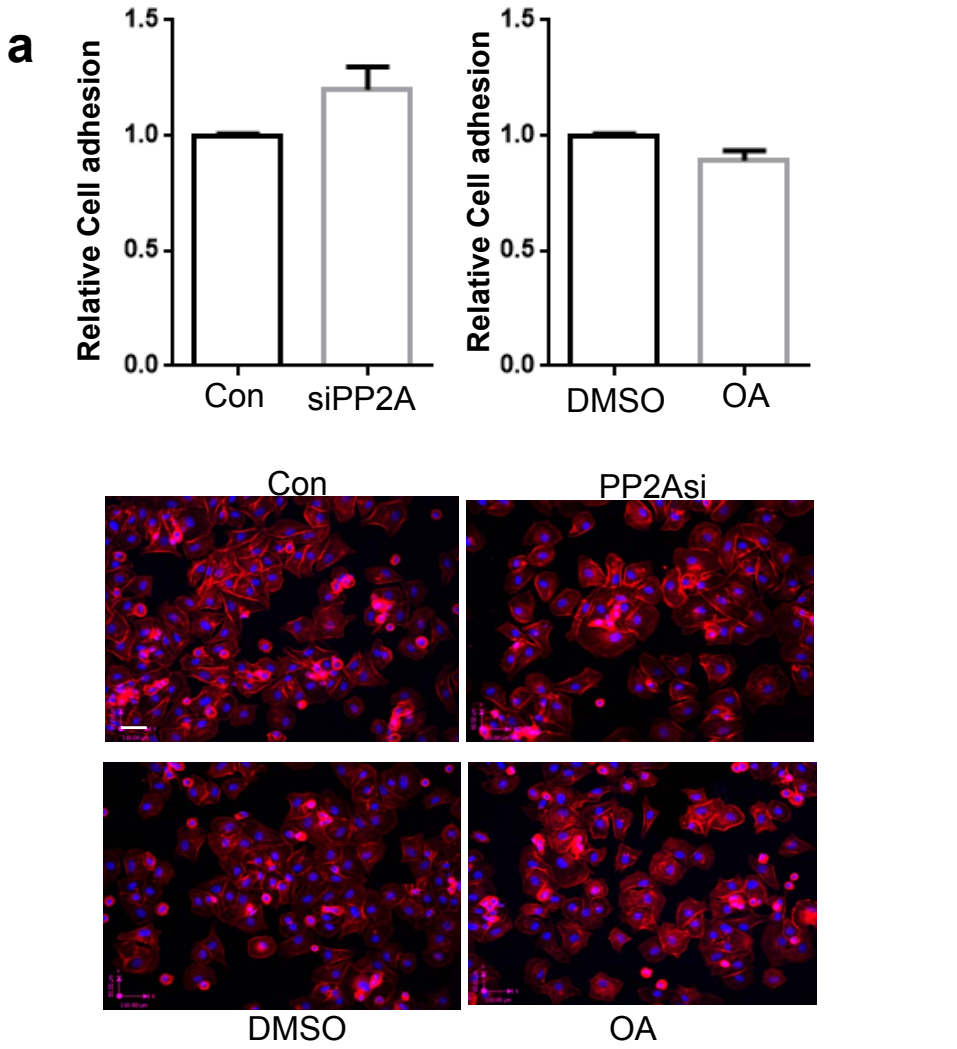

Supplementary Fig. 4

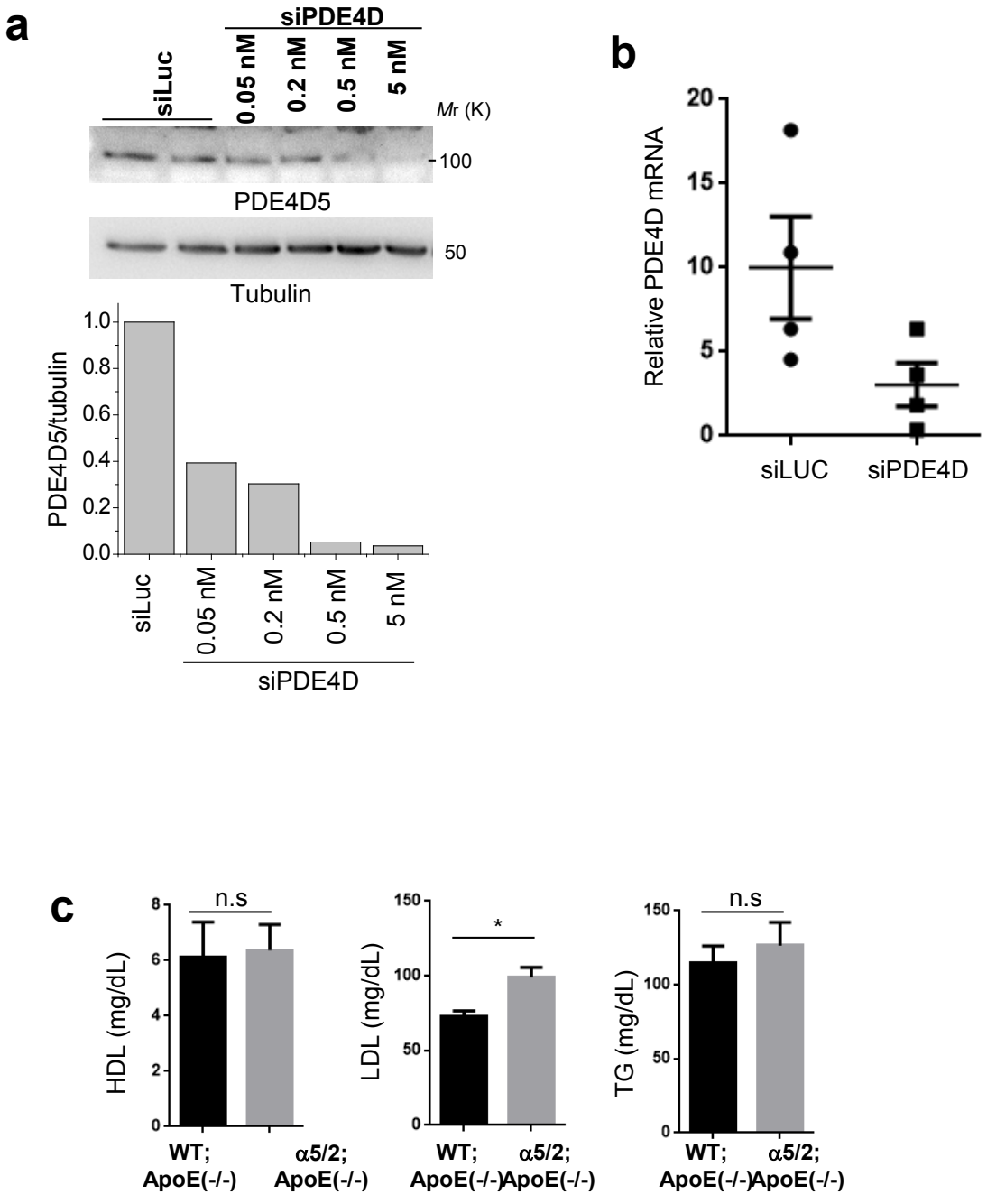

Supplementary Fig. 5